



**Ramakrishna Mission Residential College (Autonomous)**  
**Kolkata 700103, WB, India**

---

**Collaborative research in coordination chemistry of organic radicals**  
**Number 1**

**Institute 1: Ramakrishna Mission Residential College (Autonomous)**  
**Concerned Faculty: Dr. Prasanta Ghosh, Dept of Chemistry**  
**&**

**Institute 2: Max-Planck-Institut für Chemische Energiekonversion**  
Stiftstrasse 34 - 36 / D - 45470 Mülheim an der Ruhr  
**Concerned Scientist: Dr Thomas Weyhermüller**

**Period of Investigation: 20-07-2014 to 25-01-2015**


**Project: Tris(2,2'-azobispyridine) Complexes of Metal(II): X-ray Structures and Reactivities**

**Output:** The result was published in a journal of international repute

**Publication: Tris(2,2'-azobispyridine) Complexes of Copper(II): X-ray Structures, Reactivities, and the Radical Nonradical Bis(ligand) Analogues**

Suvendu Maity, Suman Kundu, Thomas Weyhermüller and Prasanta Ghosh\*

*Inorg.Chem.*, **2015**, 54, 1300-1313

  
-----  
Dr. Prasanta Ghosh

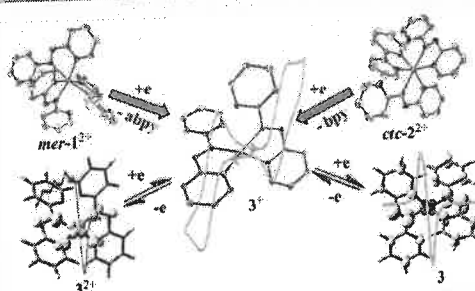
  
-----  
Dr Thomas Weyhermüller



Suvendu Maity,<sup>†</sup> Suman Kundu,<sup>†</sup> Thomas Weyhermüller,<sup>‡</sup> and Prasanta Ghosh<sup>\*†</sup>

\*Max-Planck-Institut für Chemische Energiekonversion, Stiftstrasse 34-36, D-45470 Mülheim an der Ruhr, Germany

**ABSTRACT:** Tris(abpy) complexes of types  $mer-[Cu^{II}(abpy)_3][PF_6]_2$  ( $mer-1^{2+}[PF_6^-]_2$ ) and  $ctc-[Cu^{II}(abpy)_2(bpy)][PF_6]_2$  ( $ctc-2^{2+}[PF_6^-]_2$ ) were successfully isolated and characterized by spectra and single-crystal X-ray structure determinations (abpy = 2,2'-azobispyridine; bpy = 2,2'-bipyridine). Reactions of  $mer-1^{2+}$  and  $ctc-2^{2+}$  ions with catechol, o-aminophenol, *p*-phenylenediamine, and diphenylamine (Ph-NH-Ph) in 2:1 molar ratio afford  $[Cu^I(abpy)_2]^+$  ( $3^+$ ) and corresponding quinone derivatives. The similar reactions of  $[Cu^{II}(bpy)_3]^{2+}$  and  $[Cu^{II}(phen)_3]^{2+}$  with these substrates yielding  $[Cu^I(bpy)_2]^+$  and  $[Cu^I(phen)_2]^+$  imply that these complexes undergo reduction-induced ligand dissociation reactions (phen = 1,10-phenanthroline). The average  $-N=N-$  lengths in  $mer-1^{2+}[PF_6^-]_2$  and  $ctc-2^{2+}[PF_6^-]_2$  are 1.248(4), while that in  $3^+[PF_6^-] \cdot 2CH_2Cl_2$  is relatively longer, 1.275(2) Å, due to  $d_{Cu} \rightarrow \pi_{azo}^*$  back bond reversible wave at  $-0.42$  V due to  $Cu^{II}/Cu^I$  and  $abpy/abpy^{\bullet-}$  couples:  $abpy/abpy^{\bullet-}$  couple, while those of  $ctc-2^{2+}$  ion appear at  $-0.44$ ,  $-0.86$ , and the cathodic  $3^+/3$  redox waves at  $+0.33$  and  $-0.40$  V are reversible. The functional theory (DFT) calculations authenticated the existence of  $abpy$  state of  $[Cu^I(abpy^{0.5+})(abpy^{0.5-})]$  and  $[Cu^{II}(abpy^{\bullet-})(abpy^{\bullet-})]$  states.  $[Cu^{II}(abpy)_2]^{2+}$  3 exhibits a near-IR absorption band at 2400–3000  $cm^{-1}$  transfer, elucidated by time-dependent DFT calculations in  $CH_2Cl_2$ .



isoelectronic to singlet  $^1\text{O}_2$  molecule that coordinates to biomolecules as superoxide ( $\text{O}_2^{\bullet-}$ ) and peroxide ( $\text{O}_2^{2-}$ ), exhibits similar electronic states to those of the coordinated  $\text{O}_2$  molecule. The existence of the  $-\text{N}=\text{N}-$  function of the abpy ligand in the complexes as one-electron reduced azo anion radical ( $[-\text{NN}-]^{\bullet-}$ ) and two-electron reduced hydrazido ( $[-\text{NN}-]^{2-}$ ) states were authenticated.<sup>14</sup> Note that the tris complexes of copper(II) with bidentate N,N-donor ligands are rare. Reported such complexes are  $[\text{Cu}(\text{en})_3]^{2+}$  (en = ethylenediamine),<sup>15</sup>  $[\text{Cu}(\text{bpy})_3]^{2+}$  (bpy = 2,2'-bipyridine),<sup>16</sup>  $[\text{Cu}(\text{phen})_3]^{2+}$  (phen = 1,10-phenanthroline),<sup>17</sup> and  $[\text{Cu}(\text{bpy})_2(\text{ptsb})]^{2+}$  (ptsb = *N-p*-tolylpyridine-2-aldimine).<sup>16a</sup> As the copper(II) ion in an octahedral geometry exhibits Jahn-Teller distortion, generation of tris complexes of copper(II) ion with bidentate ligands is a challenge to synthetic inorganic chemists. Moreover, tris complexes of transition metal ions with abpy, one of the stronger  $\pi$  acidic bidentate and bridging ligands,<sup>18</sup> are limited, while tris(bpy)<sup>19</sup> and tris(2-phenylazopyridine)<sup>20</sup> complexes are numerous. So far only a tris(abpy) complex of ruthenium(II) ion of type  $[\text{Ru}(\text{abpy})_3]^{2+}$  has been reported in literature.<sup>21</sup> In this work, we were successful in isolating two

The role of copper ion in biology is noteworthy. It transfers electron relatively at lower potential and exists in cytochrome *c* oxidase,<sup>1</sup> hemocyanin,<sup>2</sup> and other important electron-transfer proteins/redox enzymes such as azurin, plastocyanin, laccase, ferroxidase, tyrosinase, and ascorbate oxidase.<sup>3-7</sup> Activities of copper complexes in vitro as catalysts are vigorously encouraging.<sup>8</sup> Coordination complexes of copper that participate in redox reactions with organic substrates, are documented.<sup>9,10</sup> As the copper ion holds different geometries in different redox states, the geometry-dependent reactivities of the copper ion complexes are reported.<sup>11</sup> In this project, combination of redox-active copper(II) ion with redox noninnocent fragments, which induce new electronic states in the complexes due to redox reactions of the coordinated ligands,<sup>12</sup> was considered to be significant to develop functional molecules of copper in laboratory. The coordination complexes of copper(II) ion with the redox noninnocent ligand particularly of tris types that can participate in multielectron transfer reactions are of potential interest to establish new redox states and their reactivities.

In this work, we were persuaded to explore the tris complexes of redox noninnocent 2,2'-azobispyridine (abpy) ligand<sup>13</sup> with copper(II) ion. The  $-N=N-$  function,

Published: February 4, 2015

Table 1. Crystallographic Data for  $mer\text{-}1^{2+}[\text{PF}_6^-]_2$ ,  $ctc\text{-}2^{2+}[\text{PF}_6^-]_2$ , and  $3^+[\text{PF}_6^-]\cdot 2\text{CH}_2\text{Cl}_2$ <sup>a</sup>

	$mer\text{-}1^{2+}[\text{PF}_6^-]_2$	$ctc\text{-}2^{2+}[\text{PF}_6^-]_2$	$3^+[\text{PF}_6^-]\cdot 2\text{CH}_2\text{Cl}_2$
formula	$\text{C}_{30}\text{H}_{24}\text{CuF}_{12}\text{N}_{12}\text{P}_2$	$\text{C}_{30}\text{H}_{24}\text{CuF}_{12}\text{N}_{10}\text{P}_2$	$\text{C}_{20}\text{H}_{16}\text{CuF}_6\text{N}_8\text{P}$
fw	906.09	878.07	576.92
cryst color	black	brown	black
cryst system	monoclinic	orthorhombic	triclinic
space group	$P2_1/n$	$Pbcn$	$P\bar{1}$
a (Å)	14.1245(11)	9.9196(13)	7.3353(3)
b (Å)	14.4934(10)	22.4852(14)	12.3442(6)
c (Å)	19.195(3)	16.444(2)	12.7166(9)
$\beta$ (deg)	110.953(8)	90.00	92.653(4)
V (Å <sup>3</sup> )	3669.6(7)	3667.7(7)	1108.81(11)
Z	4	4	2
T (K)	100(2)	100(2)	100(2)
refl. collected (2 $\theta_{\text{max}}$ )	60.00	58.20	66.16
$\rho$ calcd (g cm <sup>-3</sup> )	1.640	1.590	1.728
unique refl.	79 363	45 549	16 617
ref ( $I > 2\sigma$ )	7168	3661	6914
$\mu$ (mm <sup>-1</sup> )	0.786	0.782	1.136
$\lambda$ (Å)	0.710 73	0.710 73	0.710 73
F(000)	1820	1764	580
$R1^b/\text{goodness of fit}^c$	0.0657/1.059	0.0820/1.138	0.0370/1.048
$wR2^d [I > 2\sigma(I)]$	0.1484	0.1881	0.0923
no. of params/restr.	558/186	313/164	325/0
residual density (e Å <sup>-3</sup> )	0.947/−0.530	1.123/−0.532	0.617/−1.101

<sup>a</sup>Observation criterion:  $I > 2\sigma(I)$ . <sup>b</sup> $R1 = \sum ||F_o| - |F_c|| / \sum |F_o|$ . <sup>c</sup>GOF =  $\{\sum [w(F_o^2 - F_c^2)^2] / (n - p)\}^{1/2}$ . <sup>d</sup> $wR2 = \{\sum [w(F_o^2 - F_c^2)^2] / \sum [w(F_o^2)^2]\}^{1/2}$  where  $w = 1/[\sigma^2(F_o^2) + (aP)^2 + bP]$ ,  $P = (F_o^2 + 2F_c^2)/3$ .

new tris(abpy) complexes of copper(II) ion, of types  $mer\text{-}[\text{Cu}^{\text{II}}(\text{abpy})_3][\text{PF}_6^-]_2$  ( $mer\text{-}1^{2+}[\text{PF}_6^-]_2$ ) and  $ctc\text{-}[\text{Cu}^{\text{II}}(\text{abpy})_2(\text{bpy})][\text{PF}_6^-]_2$  ( $ctc\text{-}2^{2+}[\text{PF}_6^-]_2$ ). It is observed that  $mer\text{-}1^{2+}[\text{PF}_6^-]_2$  and  $ctc\text{-}2^{2+}[\text{PF}_6^-]_2$  react with redox noninnocent organic substrates, for example, catechol, *c*-aminophenol, *p*-phenylenediamine, and diphenylamine (Ph–NH–Ph), yielding a bis(abpy) complex of copper(I) of type  $[\text{Cu}^{\text{I}}(\text{abpy})_2]^+$  ( $3^+$ ). Surprisingly, similar reduction-induced ligand dissociation reactions of the  $[\text{Cu}^{\text{II}}(\text{bpy})_3]^{2+}$  and  $[\text{Cu}^{\text{II}}(\text{phen})_3]^{2+}$  ions with the above redox noninnocent substrates are also authenticated. These reactions of copper(II) ion complexes producing copper(I) complexes are defined as reduction-induced ligand dissociation reactions. The organic substrates are oxidized by two electrons. Thus,  $mer\text{-}1^{2+}$ ,  $ctc\text{-}2^{2+}$ ,  $[\text{Cu}^{\text{II}}(\text{bpy})_3]^{2+}$ , and  $[\text{Cu}^{\text{II}}(\text{phen})_3]^{2+}$  ions parallel the activities of catecholoxidase,<sup>22</sup> aminophenoloxidase,<sup>23</sup> and amineoxidases.<sup>24</sup> In this article, syntheses, structures, and spectra of  $mer\text{-}1^{2+}[\text{PF}_6^-]_2$ ,  $ctc\text{-}2^{2+}[\text{PF}_6^-]_2$ , and  $3^+[\text{PF}_6^-]$  are reported. The ground electronic states of  $mer\text{-}1^{2+}$ ,  $ctc\text{-}2^{2+}$ ,  $3^+$ , and electrogenerated  $[\text{Cu}(\text{abpy})_2]$  (3) and  $[\text{Cu}^{\text{II}}(\text{abpy})_2]^{2+}$  ( $3^{2+}$ ) complexes were investigated by the spectroelectrochemical measurements, electron paramagnetic resonance (EPR) spectra, and density functional theory (DFT) calculations. 3 has been defined as a hybrid state of copper(II) and copper(I) ions incorporating abpy anion radical ( $\text{abpy}^{\bullet-}$ ). Origins of lower-energy electronic transitions were elucidated by quantum chemical calculations on 3,  $3^+$ , and  $3^{2+}$  ions.

## EXPERIMENTAL SECTION

**Materials and Physical Measurements.** Reagents or analytical grade materials were obtained from commercial suppliers and used without further purification. Spectroscopic grade solvents were used for spectroscopic and electrochemical measurements. The C, H, and N content of the compounds were obtained from a PerkinElmer 2400 Series II elemental analyzer. Infrared spectra of the samples were

recorded from 4000 to 400 cm<sup>-1</sup> with KBr pellets at room temperature on a PerkinElmer Spectrum RX 1 FT-IR spectrophotometer. <sup>1</sup>H NMR spectra in CDCl<sub>3</sub> solvent were recorded on a Bruker DPX 300 MHz spectrometer. Electrospray ionization (ESI) mass spectra were recorded on a micro mass Q-TOF mass spectrometer. Electronic absorption spectra in solution were recorded on a PerkinElmer Lambda 750 spectrophotometer in the range of 3300–175 nm. Magnetic susceptibilities at 298 K were recorded on a Sherwood Magnetic Susceptibility Balance. The X-band EPR spectra were recorded on a Magnettech GmbH MiniScope MS400 spectrometer (equipped with temperature controller TC H03), where the microwave frequency was measured with an FC400 frequency counter. The EPR spectra were simulated using EasySpin software. The electroanalytical instrument, BASi Epsilon-EC for cyclic voltammetric experiments in CH<sub>2</sub>Cl<sub>2</sub> solutions containing 0.2 M tetrabutylammonium hexafluorophosphate as supporting electrolyte, was used. The BASi platinum working electrode, platinum auxiliary electrode, and Ag/AgCl reference electrode were used for the measurements. The redox potential data are referenced versus ferrocenium/ferrocene, Fc<sup>+</sup>/Fc, couple. BASi SEC-C thin-layer quartz glass spectroelectrochemical cell kit (light path length of 1 mm) with platinum gauze working electrode and SEC-C platinum counter electrode were used for spectroelectrochemistry measurements.

**Syntheses. 2,2'-Azobispyridine (abpy).** This was synthesized by an oxidative coupling reaction of 2-aminopyridine using a reported procedure.<sup>13</sup>

$mer\text{-}[\text{Cu}^{\text{II}}(\text{abpy})_3][\text{PF}_6^-]_2$  ( $mer\text{-}1^{2+}[\text{PF}_6^-]_2$ ). To a solution of  $\text{Cu}(\text{NO}_3)_2 \cdot 3\text{H}_2\text{O}$  (120 mg, 0.5 mmol) in MeOH (15 mL), and CH<sub>3</sub>CN (15 mL), abpy (368 mg, 2 mmol) was added, and the solution was stirred for 48 h. A reddish-brown solution was obtained. To this brown solution, NaPF<sub>6</sub> (168 mg, 1 mmol) in MeOH (10 mL) was added, and the reaction mixture was allowed to evaporate slowly. After 2–3 d, a brown crystalline mass of  $mer\text{-}1^{2+}[\text{PF}_6^-]_2$  separated out, which was collected and dried in air. Crystals of  $mer\text{-}1^{2+}[\text{PF}_6^-]_2$  were prepared by slow diffusion of *n*-hexane to the CH<sub>2</sub>Cl<sub>2</sub> solution of the brown mass in a glass tube at 298 K (single crystals for X-ray studies were collected from this crop). Yield: 253 mg (~56% with respect to Cu). Mass spectral data [ESI, positive ion, CH<sub>3</sub>CN]: *m/z* 307.7 for  $[1^{2+}]/2$ , 615.6

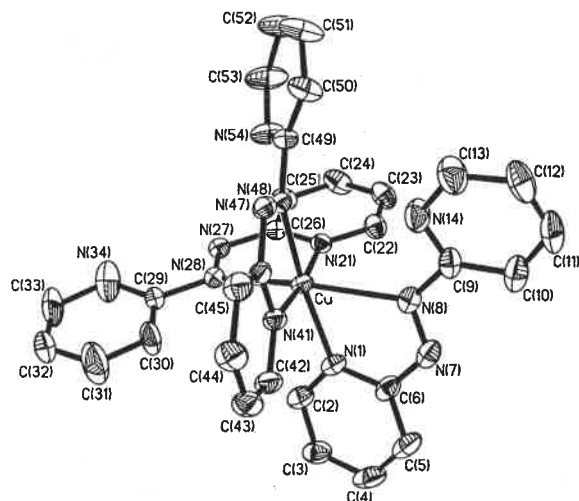


Figure 3. ORTEP plot of  $mer\text{-}1^{2+}$  with 40% thermal ellipsoids ( $\text{PF}_6^-$  ions and hydrogen atoms are omitted for clarity).

Table 3. Selected Experimental and Calculated Bond Lengths (Å) of  $mer\text{-}1^{2+}$  Ion

	experimental ( $mer\text{-}1^{2+}[\text{PF}_6^-]_2$ )	calculated $mer\text{-}1^{2+}$
Cu–N(1)	2.037(3)	2.047
Cu–N(8)	2.429(3)	2.346
Cu–N(21)	2.013(3)	2.024
Cu–N(41)	2.017(3)	2.025
Cu–N(48)	2.080(3)	2.200
Cu–N(28)	2.311(3)	2.250
N(1)–C(6)	1.347(5)	1.354
C(6)–N(7)	1.428(5)	1.406
N(7)–N(8)	1.248(4)	1.257
N(21)–C(26)	1.348(4)	1.354
C(26)–N(27)	1.419(4)	1.402
N(27)–N(28)	1.255(4)	1.256
N(41)–C(46)	1.340(4)	1.345
C(46)–N(47)	1.414(4)	1.413
N(47)–N(48)	1.251(4)	1.254

$3^+[\text{PF}_6^-] \cdot 2\text{CH}_2\text{Cl}_2$  crystallizes in the  $P\bar{1}$  space group. The molecular structure in the crystals and the atom labeling scheme are depicted in Figure 5, and the selected bond parameters are given in Table 5. The  $\text{CuN}_4$  tetrahedron is distorted. The dihedral angle ( $\varphi$ ) between two abpy planes is  $81^\circ$ . In absence of Jahn–Teller distortion that was present in  $1^{2+}[\text{PF}_6^-]_2$  and  $2^{2+}[\text{PF}_6^-]_2$ , the Cu– $\text{N}_{\text{azo}}$  distances in  $3^+[\text{PF}_6^-] \cdot 2\text{CH}_2\text{Cl}_2$  are relatively shorter. The average Cu– $\text{N}_{\text{azo}}$  lengths are 1.967(2) Å. The average Cu– $\text{N}_{\text{py}}$  lengths, 2.009(2) Å, are comparable to those observed in  $mer\text{-}1^{2+}[\text{PF}_6^-]_2$  and  $ctc\text{-}2^{2+}[\text{PF}_6^-]_2$ . The N(7)–N(8) and N(27)–N(28) azo lengths, 1.277(2) and 1.274(2) Å, are relatively longer than those found in the structure of  $1^{2+}[\text{PF}_6^-]_2$ ,  $2^{2+}[\text{PF}_6^-]_2$ , and  $[(\mu\text{-abpy})\text{-}\{\text{Cu}^+(\text{PPh}_3)_2\}][\text{PF}_6^-]_2$ .<sup>42</sup> However, the –N=N– lengths are shorter than that, 1.345(7) Å, observed in an  $\text{abcp}^{\bullet-}$  anion radical stabilized in a complex of copper(I) of type  $[(\mu\text{-abcp})\{\text{Cu}^+(\text{PPh}_3)_2\}_2][\text{PF}_6^-]$  ( $\text{abcp} = 2,2'\text{-azobis}(5\text{-chloropyrimidine})$ ) reported by Kaim et al.<sup>14c</sup>

**Electrochemical Studies.** The redox activities of  $mer\text{-}1^{2+}$ ,  $ctc\text{-}2^{2+}$ , and  $3^+$  ions in a mixture of  $\text{CH}_2\text{Cl}_2$  and  $\text{CH}_3\text{CN}$  (5:1) solvents were investigated at 298 K by cyclic voltammetry. The

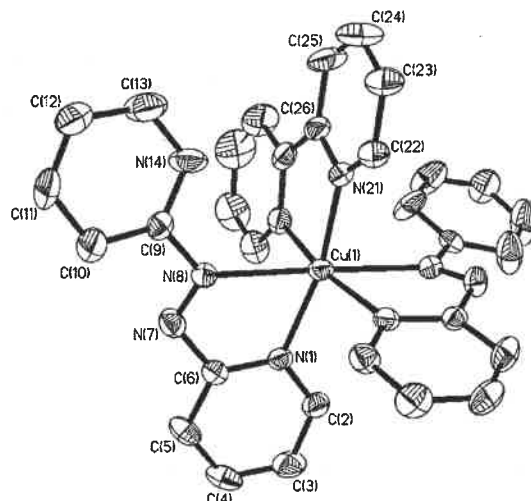


Figure 4. ORTEP plot of  $ctc\text{-}2^{2+}$  with 40% thermal ellipsoids ( $\text{PF}_6^-$  ions and hydrogen atoms are omitted for clarity).

Table 4. Selected Experimental Bond Lengths (Å) of  $ctc\text{-}2^{2+}[\text{PF}_6^-]_2$

Cu(1)–N(21)	2.004(4)
Cu(1)–N(1)	2.021(3)
Cu(1)–N(8)	2.446(3)
N(1)–C(6)	1.353(5)
C(6)–N(7)	1.423(6)
N(7)–N(8)	1.246(5)
N(8)–C(9)	1.450(7)
C(9)–N(14)	1.327(9)
N(21)–C(26)	1.344(6)
N(21)–C(22)	1.345(7)
C(13)–N(14)	1.350(9)

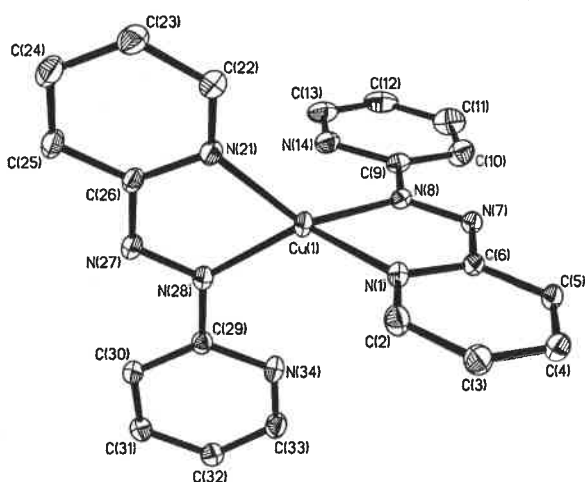


Figure 5. ORTEP plot of  $3^+$  with 40% thermal ellipsoids ( $\text{PF}_6^-$  ions,  $\text{CH}_2\text{Cl}_2$ , and hydrogen atoms are omitted for clarity).

redox potential data, referenced to ferrocenium/ferrocene ( $\text{Fc}^+/\text{Fc}$ ) couple, are summarized in Table 6. At cathode,  $mer\text{-}1^{2+}$  displays one wave at  $-0.42$  V due to the  $\text{Cu}^{2+}/\text{Cu}^+$  and  $\text{abpy}/\text{abpy}^{\bullet-}$  reduction couples and two reversible waves at  $-0.90$  and  $-1.28$  V due to the  $\text{abpy}/\text{abpy}^{\bullet-}$  couples as

Table 5. Selected Experimental Bond Lengths (Å) of  $3^+$  and Calculated Parameters of  $3^+$ ,  $3$ ,  $3^{2+}$ ,  $3^-$ , and  $[\text{Zn}(\text{abpy})_2]^+$  Using B3LYP Functional

	experimental	calculated				
	$3^+[\text{PF}_6]_2 \cdot 2\text{CH}_2\text{Cl}_2$	$3^+$	$3$	$3^{2+}$	$3^-$	$[\text{Zn}(\text{abpy})_2]^+$
M(1)–N(8)	1.963(2)	2.063	2.022	2.046	2.022	2.062
M(1)–N(28)	1.971 (2)	2.064	2.023	2.048	2.023	2.061
M(1)–N(21)	2.003(2)	2.124	2.103	2.045	2.090	2.170
M(1)–N(1)	2.017(2)	2.125	2.102	2.046	2.089	2.169
N(1)–C(2)	1.343(2)	1.338	1.341	1.339	1.377	1.343
N(1)–C(6)	1.349(2)	1.349	1.361	1.360	1.341	1.362
C(6)–N(7)	1.411(2)	1.411	1.377	1.403	1.349	1.392
N(7)–N(8)	1.277(2)	1.262	1.305	1.255	1.338	1.288
N(8)–C(9)	1.432(2)	1.423	1.401	1.414	1.379	1.393
C(9)–N(14)	1.335(2)	1.338	1.345	1.341	1.356	1.347
C(26)–N(27)	1.407(2)	1.411	1.377	1.403	1.349	1.392
N(27)–N(28)	1.274(2)	1.262	1.305	1.255	1.338	1.287
N(28)–C(29)	1.433(2)	1.423	1.402	1.415	1.379	1.393
C(29)–N(34)	1.339(2)	1.339	1.345	1.340	1.356	1.347

Table 6. Redox Potential of  $\text{mer-1}^{2+}[\text{PF}_6]_2$ ,  $\text{ctc-2}^{2+}[\text{PF}_6]_2$ , and  $3^+[\text{PF}_6]$  in  $\text{CH}_2\text{Cl}_2/\text{CH}_3\text{CN}$  (5:1) Solvent Mixture Determined by Cyclic Voltammetry at 298 K

compounds	$E_{1/2}^1$ , V ( $\Delta E^a$ , mV)	$E_{1/2}^2$ , V ( $\Delta E^a$ , mV)	$E_{1/2}^3$ , V ( $\Delta E^a$ , mV)	$E_{1/2}^4$ , V ( $\Delta E^a$ , mV)
$\text{mer-1}^{2+}[\text{PF}_6]_2$		−0.42 (300)	−0.90 (100)	−1.28 (100)
$\text{ctc-2}^{2+}[\text{PF}_6]_2$	+ 0.43 <sup>b</sup>	−0.44 (70)	−0.86 (50)	−1.10 (140)
$3^+[\text{PF}_6]$	+ 0.33 (180)	−0.40 (150)		

<sup>a</sup>Peak-to-peak separation. <sup>b</sup>Cathodic peak potential.

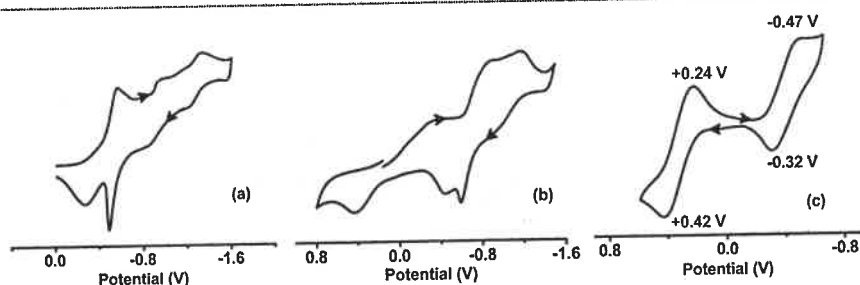


Figure 6. Cyclic voltammograms of (a)  $\text{mer-1}^{2+}[\text{PF}_6]_2$ , (b)  $\text{ctc-2}^{2+}[\text{PF}_6]_2$ , and (c)  $3^+[\text{PF}_6]$  in  $\text{CH}_2\text{Cl}_2/\text{CH}_3\text{CN}$  (5:1) solvents mixture at 298 K. Conditions: 0.2 M  $[\text{N}(\text{n-Bu})_4]\text{PF}_6$  supporting electrolyte; scan rate, 100  $\text{mV s}^{-1}$ ; platinum working electrode.

illustrated in Figure 6a. The first cathodic wave is quasi-reversible (peak-to-peak separation ( $\Delta E$ ) increases with increase of scan rate as illustrated in Supporting Information, Figure S2:  $\Delta E = 230$  mV at 50  $\text{mV sec}^{-1}$ ;  $\Delta E = 370$  mV at 400  $\text{mV sec}^{-1}$ ) and may be due to the reduction-induced ligand dissociation reaction. The  $\text{ctc-2}^{2+}$  ion exhibits these cathodic waves at −0.44, −0.86, and −1.10 V as depicted in Figure 6b. The anodic wave of  $\text{ctc-2}^{2+}$  ion at 0.43 V is irreversible. However, the redox features of  $3^+$  ion is different. Both the anodic and cathodic waves of  $3^+$  ion at +0.33 and −0.40 V are reversible as shown in Figure 6c. The EPR spectra (vide infra) of the electrogenerated  $3^{2+}$  ion and the neutral  $3$  confirm that the anodic wave is due to the  $\text{Cu}^{2+}/\text{Cu}^+$  couple, while the cathodic wave is due to the  $\text{abpy}/\text{abpy}^{\bullet-}$  couple.

**EPR Spectra.** Magnetic susceptibility measurements at 298 K confirmed the one-electron paramagnetism of  $\text{mer-1}^{2+}[\text{PF}_6]_2$  and  $\text{ctc-2}^{2+}[\text{PF}_6]_2$  complexes. X-band EPR spectra of the frozen  $\text{CH}_2\text{Cl}_2$  glasses (123 K) of  $\text{mer-1}^{2+}[\text{PF}_6]_2$  and  $\text{ctc-2}^{2+}[\text{PF}_6]_2$  were recorded. The spectra with simulations are illustrated in Figure 7, and the EPR parameters are summarized in Table 7.

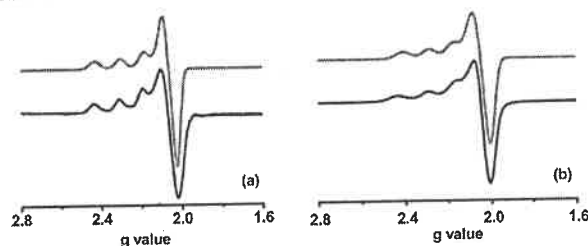


Figure 7. X-band EPR spectra of the frozen  $\text{CH}_2\text{Cl}_2$  glasses of (a)  $\text{mer-1}^{2+}[\text{PF}_6]_2$  and (b)  $\text{ctc-2}^{2+}[\text{PF}_6]_2$  (black, experimental; red, simulated) at 123 K.

The axial EPR spectra of  $\text{mer-1}^{2+}[\text{PF}_6]_2$  and  $\text{ctc-2}^{2+}[\text{PF}_6]_2$  are similar. The spectra exhibit hyperfine structures due to  $^{63,65}\text{Cu}$  nuclei. The simulated  $g$  parameters are  $\text{mer-1}^{2+}$ ,  $g_1 = 2.062$ ,  $g_2 = 2.245$ ;  $\text{ctc-2}^{2+}$ ,  $g_1 = 2.043$ ,  $g_2 = 2.233$ , which are consistent with those reported for copper(II) complexes.<sup>43</sup> The EPR spectrum of the frozen  $\text{CH}_2\text{Cl}_2$  glass of  $3^{2+}$  at 123 K with simulation is shown in Figure 8a. The hyperfine structured spectrum with  $g_1$

## Inorganic Chemistry

for  $[1]^{2+}$ . Anal. Calcd (%) for  $C_{30}H_{24}CuF_{12}N_{12}P_2$ : C, 59.53; H, 4.39; N, 5.55; Found: C, 59.33; H, 4.44; N, 5.41. IR,  $cm^{-1}$  (KBr):  $\nu$  3401 (br), 1631 (m), 1578 (vs), 1559 (vs), 1444 (vs), 1416 (s), 1313 (m), 1250 (m), 1040 (m), 1016 (m), 835 (vs), 779 (vs), 758 (vs), 737 (m).

$ctc-[Cu^{II}(abpy)_2(bpy)][PF_6]_2$  ( $ctc-2^{2+}[PF_6]_2$ ). The bluish-white  $[Cu^{II}(bpy)Cl_2]$  was prepared by a reported procedure.<sup>25</sup> To a solution of  $[Cu^{II}(bpy)Cl_2]$  (145 mg, 0.5 mmol) in MeOH (15 mL), solid  $AgNO_3$  (168 mg, 1 mmol) was added and stirred for 30 min, and the reaction mixture was filtered. A white residue of  $AgCl$  was discarded. To the blue filtrate, abpy (184 mg, 1 mmol) was added, and the mixture was stirred for 30 min. The solution turned brown, which was filtered. To the filtrate a solution of  $NaPF_6$  (168 mg, 1 mmol) in MeOH (5 mL) was added, and the solution was allowed to evaporate slowly at 298 K. After 4–5 d, deep brown crystals of  $ctc-2^{2+}[PF_6]_2$  separated out, which were filtered and dried in air. Yield: 310 mg (~71% with respect to Cu). Mass spectral data [ESI, positive ion,  $CH_3CN$ ]:  $m/z$  293.07 for  $[2^{2+}]_2$ , 587.0 for  $[2]^{2+}$ . Anal. Calcd (%) for  $C_{30}H_{24}CuF_{12}N_{10}P_2$ : C, 61.27; H, 4.11; N, 23.82; Found: C, 61.21; H, 3.99; N, 23.72. IR,  $cm^{-1}$  (KBr):  $\nu$  3421 (br), 1685 (m), 1631 (m), 1600 (vs), 1577 (s), 1566 (s), 1472 (s), 1444 (vs), 1313 (m), 1158 (m), 1060 (m), 1026 (s), 830 (vs), 766 (vs), 730 (s).

$[Cu^{II}(abpy)_2][PF_6]$  ( $3^+[PF_6]$ ). To  $mer-1^{2+}[PF_6]_2$  (226 mg, 0.25 mmol) or  $ctc-2^{2+}[PF_6]_2$  (219 mg, 0.25 mmol) in  $CH_2Cl_2$  (20 mL), a solution of catechol (13.8 mg, 0.125 mmol) in  $CH_2Cl_2$  (10 mL) was added. The brown solution turned deep violet instantaneously. The solution was evaporated under vacuum, and residue was washed twice with diethyl ether to remove excess catechol, *o*-quinone, and dissociated abpy (in case of  $mer-1^{2+}[PF_6]_2$ ) or bpy (in case of  $ctc-2^{2+}[PF_6]_2$ ) ligands. The residue was dissolved in minimum volume of  $CH_2Cl_2$  (~10 mL), which was allowed to evaporate in air at 298 K. After 3–4 d, violet crystals of  $3^+[PF_6]_2 \cdot 2CH_2Cl_2$  separated, which were collected and dried in air. Yield: 202 mg (~82% with respect to Cu). Mass spectral data [ESI, positive ion,  $CH_3CN$ ]:  $m/z$  431 for  $[3]^+$ . Anal. Calcd (%) for  $C_{20}H_{16}CuF_6N_8P_2$ : C, 55.61; H, 3.73; N, 25.94; Found: C, 55.57; H, 3.62; N, 25.80.  $^1H$  NMR ( $CDCl_3$ , 300 MHz, 298 K):  $\delta$  (ppm) = 8.83 (d, 2H), 8.28 (t, 2H), 8.13 (d, 2H), 7.84 (t, 2H), 7.65–7.52 (br, 4H), 7.05–7.03 (br, 4H). IR,  $cm^{-1}$  (KBr):  $\nu$  3424 (br), 1646 (m), 1599 (m), 1580 (m), 1470 (s), 1431 (s), 1375 (m), 1271 (m), 835 (vs), 794 (s), 575 (s).

$[Cu^{II}(abpy)_2]^{2+}$  ( $3^{2+}$ ) and  $[Cu(abpy)_2]$  ( $3$ ).  $3^{2+}$  and  $3$  complexes were not isolated in this search. However, these complexes were generated coulometrically for spectroelectrochemical measurements and EPR spectral analyses.

**Single-Crystal X-ray Structure Determinations of the Complexes.** Dark single crystals of  $mer-1^{2+}[PF_6]_2$ ,  $ctc-2^{2+}[PF_6]_2$ , and  $3^+[PF_6]_2 \cdot 2CH_2Cl_2$  were picked up with nylon loops and were mounted on a Bruker APEX-II CCD diffractometer (at 100 K) equipped with a Mo-target rotating-anode X-ray source and a graphite monochromator (Mo  $K\alpha$ ,  $\lambda = 0.71073$  Å). Final cell constants were obtained from least-squares fits of all measured reflections. Intensity of data was corrected for absorption using intensities of redundant reflections. The structures were readily solved by direct methods and subsequent difference Fourier techniques. The crystallographic data of  $mer-1^{2+}[PF_6]_2$ ,  $ctc-2^{2+}[PF_6]_2$ , and  $3^+[PF_6]_2 \cdot 2CH_2Cl_2$  are listed in Table 1. The Siemens SHELXS-97<sup>26</sup> software package was used for solution, and SHELXL-97<sup>27</sup> was used for the refinement. All non-hydrogen atoms were refined anisotropically. Hydrogen atoms were placed at the calculated positions and refined as riding atoms with isotropic displacement parameters.

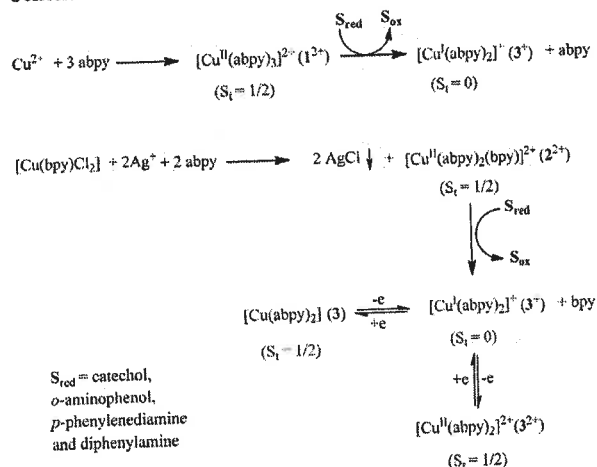
**Density Functional Theory Calculations.** All calculations reported in this article were done with the Gaussian 03W<sup>28</sup> program package supported by GaussView 4.1. The DFT<sup>29</sup> and time-dependent (TD) DFT<sup>30</sup> calculations were performed at the level of Becke three parameter hybrid functional with the nonlocal correlation functional of Lee–Yang–Parr (B3LYP).<sup>31</sup> Gas-phase geometries of  $mer-1^{2+}$ ,  $fac-[Cu^{II}(abpy)_3]^{2+}$ ,  $ctc-[Cu^{II}(abpy)_2(bpy)]^{2+}$  ( $ctc-2^{2+}$ ),  $ccc-[Cu^{II}(abpy)_2(bpy)]^{2+}$ ,  $[Cu(abpy)_2]$  ( $3$ ),  $[Cu^{II}(abpy)_2]^{2+}$  ( $3^{2+}$ ), and  $[Zn(abpy)_2]^+$  were optimized with doublet spin state, while  $[Cu^I(abpy)_2]^+$  ( $3^+$ ) and  $[Cu(abpy)_2]^-$  ( $3^-$ ) ions were optimized with singlet spin state using Pulay's Direct

Inversion<sup>32</sup> in the Iterative Subspace (DIIS), "tight" convergent self-consistent field procedure<sup>33</sup> ignoring symmetry. In all calculations, a LANL2DZ basis set along with the corresponding effective core potential was used for copper metal.<sup>34</sup> Valence double- $\zeta$  basis set, 6-31G<sup>35</sup> for H was used. For C and N non-hydrogen atoms valence double- $\zeta$  with diffuse and polarization functions, 6-31++G\*\* as basis set<sup>36</sup> was employed for all calculations. The percentage contributions of metal and ligands to the frontier orbitals were calculated using GaussSum program package.<sup>37</sup> The 60 lowest singlet excitation energies on each of the optimized geometries of  $3^+$ ,  $3^{2+}$ , and  $3$  in  $CH_2Cl_2$  using CPCM model<sup>38</sup> were calculated by TD DFT method. The natures of transitions were calculated by adding the probability of same type among  $\alpha$  and  $\beta$  molecular orbitals. The magnetic coupling constant ( $J$ ) of  $[Cu^{II}(abpy^+)(abpy^+)]$  state of  $3$  was calculated using Yamaguchi approach.<sup>39</sup> Energy of the high-spin quartet state of  $3$  was calculated on the optimized geometry of the doublet state of  $3$ .

## RESULTS

**Syntheses and Characterizations.** Tris(abpy) and bis(abpy) complexes of copper(II) and copper(I) ions isolated and investigated in this work are summarized in Scheme 1.

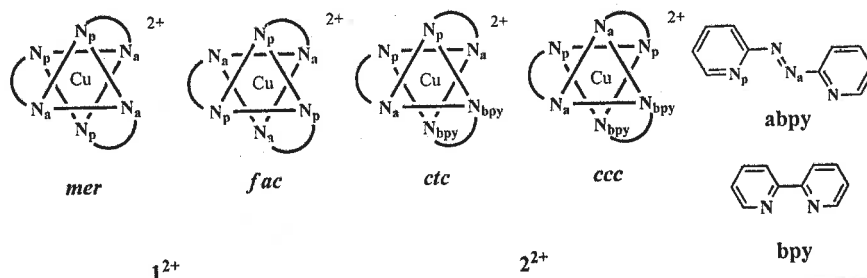
Scheme 1



Details of the syntheses of the complexes are outlined in the Experimental Section;  $mer-1^{2+}$  was synthesized by a reaction of cupric ion with excess abpy ligand, while  $ctc-2^{2+}$  was synthesized by a reaction of  $[Cu^{II}(bpy)Cl_2]$  with 2 equiv of  $Ag^+$  ion followed by abpy ligand. Because of the coordination of two nonequivalent azo- and pyridine nitrogen atoms, the geometrical isomerizations of the azopyridine complexes of transition metal ions are common.<sup>40</sup> The mer and fac, the two geometrical isomers of  $1^{2+}$  ion and ctc and ccc isomers of  $2^{2+}$  ion, are shown in Chart 1 (ctc refers to cis–trans–cis positions of pyridine–azo–bipyridine nitrogen atoms; ccc refers to cis–cis–cis positions of pyridine–azo–bipyridine nitrogen atoms). In this work, we were successful in isolating the mer isomer of  $1^{2+}$ . No fac isomer was detected.

Similar observations were reported in cases of the tris(2-phenylazopyridine) complexes of ruthenium(II) ion,<sup>40a</sup> while the fac isomers were isolated with rhenium(I) ion.<sup>40d,e</sup> However, both fac and mer isomers of tris(abpy) complexes of ruthenium(II) ion were successfully isolated.<sup>21</sup> In case of  $2^{2+}$  ion, we succeeded to isolate only the ctc isomer. The stability of mer and fac isomers of  $1^{2+}$  and ctc and ccc isomers of  $2^{2+}$  ion were analyzed by DFT calculations (vide infra).

Chart 1



Both *mer*-1<sup>2+</sup> and *ctc*-2<sup>2+</sup> react with redox noninnocent catechol, *o*-aminophenol, *p*-phenylenediamine, and diphenylamine producing 3<sup>+</sup> ion. In this work, the cations were isolated as *mer*-1<sup>2+</sup>[PF<sub>6</sub>]<sub>2</sub>, *ctc*-2<sup>2+</sup>[PF<sub>6</sub>]<sub>2</sub>, and 3<sup>+</sup>[PF<sub>6</sub>]<sub>2</sub> complex salts, while the neutral complex 3 and 3<sup>2+</sup> ion were generated coulometrically for spectroelectrochemical measurements and EPR spectra; *mer*-1<sup>2+</sup>[PF<sub>6</sub>]<sub>2</sub>, *ctc*-2<sup>2+</sup>[PF<sub>6</sub>]<sub>2</sub>, and 3<sup>+</sup>[PF<sub>6</sub>]<sub>2</sub> were characterized by elemental analyses and spectral data. Molecular geometries in crystals were confirmed by single-crystal X-ray structure determinations (vide infra) of *mer*-1<sup>2+</sup>[PF<sub>6</sub>]<sub>2</sub>, *ctc*-2<sup>2+</sup>[PF<sub>6</sub>]<sub>2</sub>, and 3<sup>+</sup>[PF<sub>6</sub>]<sub>2</sub>·2CH<sub>2</sub>Cl<sub>2</sub>.

The reductions of *mer*-1<sup>2+</sup> and *ctc*-2<sup>2+</sup> by organic substrates were investigated by UV–vis spectra. UV–vis–NIR absorption spectra of *mer*-1<sup>2+</sup>[PF<sub>6</sub>]<sub>2</sub>, *ctc*-2<sup>2+</sup>[PF<sub>6</sub>]<sub>2</sub>, and 3<sup>+</sup>[PF<sub>6</sub>]<sub>2</sub> were recorded in CH<sub>2</sub>Cl<sub>2</sub> at 298 K. The spectra are shown in Figure 1, and the data are summarized in Table 2. *Mer*-1<sup>2+</sup> and *ctc*-2<sup>2+</sup>

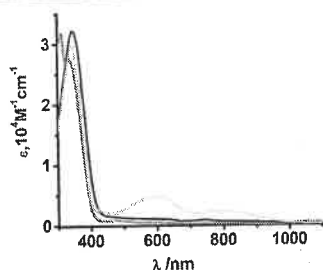


Figure 1. Electronic spectra of *mer*-1<sup>2+</sup>[PF<sub>6</sub>]<sub>2</sub> (black), *ctc*-2<sup>2+</sup>[PF<sub>6</sub>]<sub>2</sub> (red), and 3<sup>+</sup>[PF<sub>6</sub>]<sub>2</sub> (green) in CH<sub>2</sub>Cl<sub>2</sub> solution at 298 K.

Table 2. Electronic Absorption Spectral Data of *mer*-1<sup>2+</sup>[PF<sub>6</sub>]<sub>2</sub>, *ctc*-2<sup>2+</sup>[PF<sub>6</sub>]<sub>2</sub>, and 3<sup>+</sup>[PF<sub>6</sub>]<sub>2</sub> in CH<sub>2</sub>Cl<sub>2</sub> at 298 K

complexes	λ <sub>max</sub> nm (ε, 1 × 10 <sup>4</sup> M <sup>-1</sup> cm <sup>-1</sup> )
<i>mer</i> -1 <sup>2+</sup> [PF <sub>6</sub> ] <sub>2</sub>	744 (0.07) <sup>sh</sup> , 578 (0.10) <sup>sh</sup> , 346 (3.22)
<i>ctc</i> -2 <sup>2+</sup> [PF <sub>6</sub> ] <sub>2</sub>	622 (0.04) <sup>sh</sup> , 464 (0.09) <sup>sh</sup> , 340 (2.27), 314 (3.18)
3 <sup>+</sup> [PF <sub>6</sub> ] <sub>2</sub>	806 (0.20), 597 (0.40), 346 (2.90)
3	2744 (1.21), 2729 (1.20), 2599 (0.319), 1049 (0.103), 713 (0.28), 604 (0.39)
3 <sup>2+</sup>	818 (0.14), 599 (0.72), 344 (3.61)

do not display any lower-energy absorption band, while 3<sup>+</sup> ion absorbs significantly at 806 and 597 nm. The conversions of *mer*-1<sup>2+</sup> and *ctc*-2<sup>2+</sup> to 3<sup>+</sup> in the presence of organic reducing agents were monitored by these two absorption maxima.

To a solution of *mer*-1<sup>2+</sup>[PF<sub>6</sub>]<sub>2</sub> in CH<sub>2</sub>Cl<sub>2</sub> (2.5 mL, 0.80 × 10<sup>-4</sup> M/lit) in a quartz cell, a solution of catechol in CH<sub>2</sub>Cl<sub>2</sub> (4.1 × 10<sup>-4</sup> M) was added dropwise, and the change of the absorption spectrum of the cations was recorded as shown in Figure 2a. The catechol solution was added until a constant

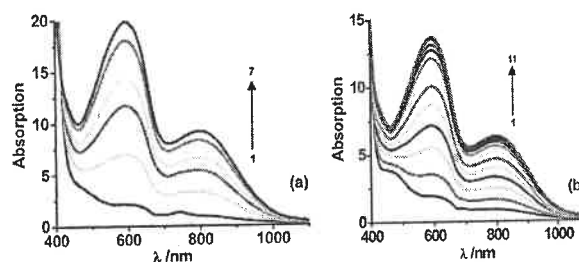


Figure 2. Change of electronic spectra during the reactions of (a) *mer*-1<sup>2+</sup>[PF<sub>6</sub>]<sub>2</sub> and (b) *ctc*-2<sup>2+</sup>[PF<sub>6</sub>]<sub>2</sub> with catechol in CH<sub>2</sub>Cl<sub>2</sub> at 298 K.

absorption maximum was obtained. It was calculated that the complex *mer*-1<sup>2+</sup>[PF<sub>6</sub>]<sub>2</sub> and the catechol required for the titration were in a molar ratio of 2:1, affirming two-electron oxidation of catechol to *o*-quinone. The similar reaction of *ctc*-2<sup>2+</sup>[PF<sub>6</sub>]<sub>2</sub> with catechol was authenticated by recording the spectral change during the reaction as depicted in Figure 2b. The redox reactions of *mer*-1<sup>2+</sup>[PF<sub>6</sub>]<sub>2</sub> and *ctc*-2<sup>2+</sup>[PF<sub>6</sub>]<sub>2</sub> with *o*-aminophenol, *p*-phenylenediamine, and diphenylamine were similarly followed by UV–vis absorption spectra, which are illustrated in Figure S1 (Supporting Information). In every case, the product is 3<sup>+</sup> ion.

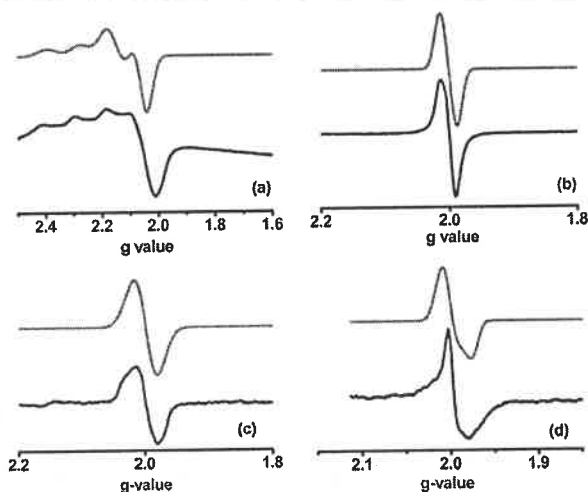
**Molecular Geometries.** Single-crystal X-ray structure determinations of *mer*-1<sup>2+</sup>[PF<sub>6</sub>]<sub>2</sub>, *ctc*-2<sup>2+</sup>[PF<sub>6</sub>]<sub>2</sub>, and 3<sup>+</sup>[PF<sub>6</sub>]<sub>2</sub>·2CH<sub>2</sub>Cl<sub>2</sub> confirmed the molecular geometries of these three types of complexes in crystals; *mer*-1<sup>2+</sup>[PF<sub>6</sub>]<sub>2</sub> crystallizes in the P2<sub>1</sub>/n space group. The molecular structure in the crystals and the atom labeling scheme of *mer*-1<sup>2+</sup>[PF<sub>6</sub>]<sub>2</sub> are illustrated in Figure 3, and the selected bond parameters are listed in Table 3. The CuN<sub>6</sub> octahedron is severely distorted where two Cu–N<sub>azo</sub> bonds, namely, Cu–N(8) and Cu–N(28), are elongated. The average Cu–N<sub>py</sub> lengths are 2.022(3) Å, while the trans Cu–N(8) and Cu–N(28) bonds are 2.429(3) and 2.311(3) Å, respectively. The feature is defined by the static Jahn–Teller distortion.<sup>41</sup> The three –N=N– lengths, N(7)–N(8), N(27)–N(28), and N(47)–N(48), respectively, are 1.248(4), 1.255(4), and 1.251(4) Å.

Complex *ctc*-2<sup>2+</sup>[PF<sub>6</sub>]<sub>2</sub> crystallizes in the *Pbcn* space group. The molecular structure in the crystal and the atom labeling scheme are shown in Figure 4, and the selected bond parameters are summarized in Table 4. The gross geometry of *ctc*-2<sup>2+</sup> ion is similar to that of *mer*-1<sup>2+</sup> ion, only one of the *abpy* ligands of *mer*-1<sup>2+</sup> ion is replaced by a *bpy* ligand in *ctc*-2<sup>2+</sup> ion. The CuN<sub>6</sub> octahedron exhibits an axial Jahn–Teller distortion along trans Cu–N<sub>azo</sub> bonds. The Cu<sup>II</sup>–N<sub>azo</sub> distance is 2.446(3) Å, while the average Cu<sup>II</sup>–N<sub>py</sub> lengths are 2.012(4) Å. The average –N=N– lengths are 1.246(5) Å.



Table 7. X-Band EPR Spectral Parameters of  $mer\text{-}1^{2+}[\text{PF}_6^-]_2$ ,  $2^{2+}[\text{PF}_6^-]_2$ ,  $3^{2+}$ , and 3

comp	conditions	temp (K)	$g_{\text{iso}}/g_{\text{av}}$	$g_1$	$g_2$	$\Delta g^a$	A (G)
$mer\text{-}1^{2+}[\text{PF}_6^-]_2$	$\text{CH}_2\text{Cl}_2$ frozen glass	123	2.153	2.062	2.245	0.183	$^{63,65}\text{Cu}$ ( $A_1 = 16$ , $A_2 = 159$ )
$ctc\text{-}2^{2+}[\text{PF}_6^-]_2$	$\text{CH}_2\text{Cl}_2$ frozen glass	123	2.138	2.043	2.233	0.190	$^{63,65}\text{Cu}$ ( $A_1 = 19$ , $A_2 = 153$ )
$3^{2+}$	$\text{CH}_2\text{Cl}_2$ frozen glass	123	2.166	2.105	2.228	0.123	$^{63,65}\text{Cu}$ ( $A_1 = 42$ , $A_2 = 146$ )
3	Solid	298	2.001				$^{14}\text{N}$ ( $A = 14$ )
	$\text{CH}_2\text{Cl}_2$ solution	298	2.001				$^{14}\text{N}$ ( $A_1 = 8$ , $A_2 = 16$ )
	$\text{CH}_2\text{Cl}_2$ frozen glass	123	1.999	1.999	1.999		

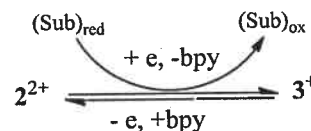
Figure 8. X-band EPR spectra of (a)  $3^{2+}$ , frozen  $\text{CH}_2\text{Cl}_2$  glass at 123 K; (b) 3, solid state at 298 K; (c) 3,  $\text{CH}_2\text{Cl}_2$  at 298 K; (d) 3, frozen  $\text{CH}_2\text{Cl}_2$  glass at 123 K (black, experimental; red, simulated).

$= 2.105$  and  $g_2 = 2.228$  correlates well to the existence of copper(II) ion in  $3^{2+}$  ion, while the EPR spectra in solid (298 K),  $\text{CH}_2\text{Cl}_2$  solution (298 K), and  $\text{CH}_2\text{Cl}_2$  frozen glass (123 K) established the existence of organic radical in 3. The spectra with the simulations are depicted in Figure 8. The spectrum of 3 in solid is sharper (Figure 8b), and the simulated  $g$  value is 2.001. In solution and frozen glass, the spectra with  $g = 2.001$  and 1.999 are relatively broader, as illustrated in Figure 8c,d, due to the coupling of the azo nitrogen atoms. The coupling constants ( $A$ ) are listed in Table 7. The frozen glass EPR spectrum was simulated with  $g_1 = g_2 = 1.999$ ;  $A_{1(\text{N})} = 8$ ,  $A_{2(\text{N})} = 16$  G. It unambiguously inferred that 3 incorporates an  $\text{abpy}^{\bullet-}$  anion radical coordinated to copper(I) ion. However, as  $3^+$  displays only one  $\text{abpy}/\text{abpy}^{\bullet-}$  reduction wave at cathode, both the  $\text{abpy}$  ligands are equally reduced, and on the basis of these data, 3 is defined as a copper(I) complex of type  $[\text{Cu}^{\text{I}}(\text{abpy}^{0.5\bullet-})_2(\text{abpy}^{0.5\bullet-})]$  (vide infra).<sup>44</sup>

This EPR spectrum of  $\text{CH}_2\text{Cl}_2$  frozen glass of  $3^{2+}$  is significantly different from those of  $mer\text{-}1^{2+}$  and  $ctc\text{-}2^{2+}$  ions. The spectral parameters corroborate well with those reported in cases of distorted square planar complexes of copper(II) ion.<sup>45</sup> The  $3^{2+}$  ion reacts with excess  $\text{bpy}$  ligand. The EPR spectrum of  $3^{2+}$  ion in the presence of excess  $\text{bpy}$  was recorded. The spectrum is similar to that of  $ctc\text{-}2^{2+}$  (Figure 7b) ion authenticating the conversion of  $3^{2+}$  ion to  $2^{2+}$  ion. It predicts the reversibility of the transformation of  $1^{2+}$  and  $2^{2+}$  ions to  $3^+$  ion and vice versa as given in Scheme 2.

**Density Functional Theory Calculations.** In conjunction with the X-ray bond parameters and the spectral data, the DFT calculations were performed to elucidate the electronic

Scheme 2



structures of  $mer\text{-}1^{2+}$ ,  $ctc\text{-}2^{2+}$ ,  $3^+$ ,  $3^{2+}$ , 3, and  $3^-$ . The gas-phase geometries of  $mer$  and  $fac$  isomers of  $1^{2+}$  ion,  $ctc$ , and  $ccc$  isomers of  $2^{2+}$  ion,  $3^{2+}$  ion, 3, and  $[\text{Zn}(\text{abpy})_2]^+$  were optimized with the doublet spin state, while the gas-phase geometries of  $3^+$  and  $3^-$  ions were optimized with the singlet spin state. Optimized geometries are shown in Supporting Information, Figure S3. The calculated bond parameters of  $mer\text{-}1^{2+}$  and  $ctc\text{-}2^{2+}$  ions are listed in Tables 3 and 4, and those of  $3^+$ ,  $3^{2+}$ , 3,  $3^-$ , and  $[\text{Zn}(\text{abpy})_2]^+$  are summarized in Table 5.

**$mer\text{-}[\text{Cu}^{\text{II}}(\text{abpy})_2]^{2+}$  ( $mer\text{-}1^{2+}$ ) and  $fac\text{-}[\text{Cu}^{\text{II}}(\text{abpy})_2]^{2+}$  ( $fac\text{-}1^{2+}$ ) Isomers.** The DFT calculations on  $mer$ - and  $fac\text{-}1^{2+}$  isomers disclose the trend of the relative ground state energies of the  $mer$  and  $fac$  isomers of the tris(azopyridine) complexes of the transition metal ions. The calculations authenticated that the ground state of the  $mer\text{-}1^{2+}$  ion, which was isolated experimentally, is more stable than that of the  $fac$  isomer by 23 kJ/mol. The calculated bond parameters of  $mer\text{-}1^{2+}$  ion compare well to those obtained from the single-crystal X-ray structure determination of  $mer\text{-}1^{2+}[\text{PF}_6^-]_2$ . The calculated average  $\text{N}=\text{N}$  lengths are 1.256 Å, which implies the coordination of neutral  $\text{abpy}$  ligand to the copper(II) ion. Mulliken spin density is expectedly localized on the copper ion as shown in Figure 9a.

**$ctc\text{-}[\text{Cu}^{\text{II}}(\text{abpy})_2(\text{bpy})]^{2+}$  ( $ctc\text{-}2^{2+}$ ) and  $ccc\text{-}[\text{Cu}^{\text{II}}(\text{abpy})_2(\text{bpy})]^{2+}$  ( $ccc\text{-}2^{2+}$ ) Isomers.** Both  $ctc$  and  $ccc$  isomers of the bis(azopyridine) complexes of type  $[\text{M}(\text{azopyridine})_2\text{X}_2]$  were reported in many cases. In this work, to analyze the stabilities of these two isomers, gas-phase geometries of  $ctc\text{-}2^{2+}$  and  $ccc\text{-}2^{2+}$  isomers were optimized. The calculations infer that in gas phase the  $ctc\text{-}2^{2+}$  is stabilized by 9.6 kJ/mol more than the  $ccc\text{-}2^{2+}$  ion. Experimentally, we were successful in isolating  $ctc\text{-}2^{2+}$  isomer only. The calculated bond parameters of  $ctc\text{-}2^{2+}$  ion are similar to those obtained from the single-crystal X-ray structure determination of  $ctc\text{-}2^{2+}[\text{PF}_6^-]_2$ . The average  $\text{N}=\text{N}$  lengths are 1.256 Å. The Mulliken spin density of  $ctc\text{-}2^{2+}$  ion is localized on the copper ion as observed in case of  $mer\text{-}1^{2+}$  ion and is shown in Figure 9b.

**$[\text{Cu}^{\text{I}}(\text{abpy})_2]^+$  ( $3^+$ ).** The  $3^+$  ion exhibits a distorted tetrahedral geometry. The dihedral angle between two  $\text{abpy}$  ligands is  $81^\circ$  as shown in Chart 2a. In crystals it is  $80^\circ$  determined by single-crystal X-ray structure determination of  $3^+[\text{PF}_6^-]_2 \cdot 2\text{CH}_2\text{Cl}_2$ . The closed cell singlet (CSS) solution of  $3^+$  ion is stable confirming the coordination of neutral  $\text{abpy}$  ligand to the copper(I) ion. The calculated bond parameters are listed in Table 5. The calculated lengths correlate well to those obtained from the X-

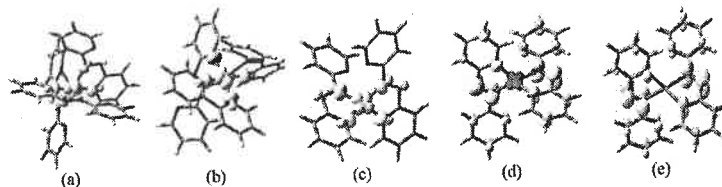


Figure 9. Spin density plots (yellow,  $\alpha$  spin; red,  $\beta$  spin) and values from Mulliken spin population analyses [atomic spin densities] of (a)  $mer\text{-}1^{2+}$  [Cu(1) 0.57, N(8) 0.08, N(21) 0.10, N(41) 0.11]. (b)  $ctc\text{-}2^{2+}$  [Cu(1) 0.55, N(1) 0.10, N(21) 0.11, N(21A) 0.12, N(1A) 0.11]. (c)  $3^{2+}$  [Cu(1) 0.50, N(1) 0.08, N(9) 0.13, N(21) 0.08, N(28) 0.13]. (d) **3** [Cu(1) -0.22, C(2) -0.02, C(6) -0.02, C(9) -0.08, C(29) -0.08, C(33) -0.03, N(1) 0.06, N(7) 0.22, N(8) 0.15, N(14) 0.05, C(3) 0.09, C(5) 0.06, C(10) 0.10, C(12) 0.08, N(21) 0.06, C(23) 0.09, C(25) 0.06, N(27) 0.22, C(32) 0.08]. (e)  $[Zn(abpy)_2]^+$  [N(1) 0.06, N(7) 0.18, N(8) 0.14, C(10) 0.06, C(12) 0.06, N(21) 0.06, C(23) 0.07, N(27) 0.18, N(28) 0.14].

Chart 2. Calculated Dihedral Angle ( $\varphi$ ) between the Planes of Two abpy Ligands in  $3^{2+}$ ,  $3^+$ , **3**, and  $3^-$

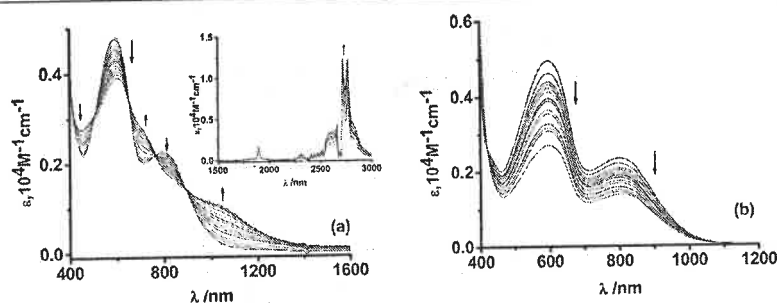
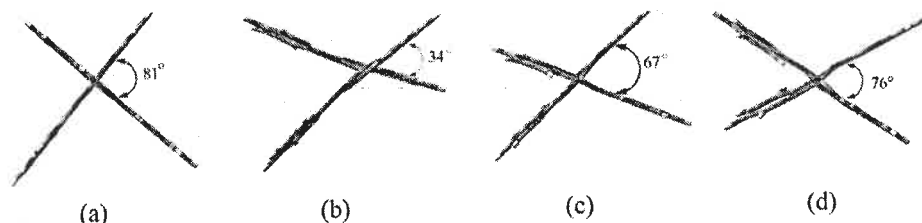


Figure 10. Spectroelectrochemistry of (a)  $[3^+ \rightarrow 3]$  and (b)  $[3^+ \rightarrow 3^{2+}]$  in  $CH_2Cl_2$  at 298 K. (inset) NIR absorption bands.

ray structure of  $3^+ [PF_6]_2 \cdot 2CH_2Cl_2$ . The relatively longer  $-N=N-$  lengths, 1.262 Å, compared to those in  $1^{2+} [PF_6]_2$  and  $2^{2+} [PF_6]_2$  are due to the mixing of  $d_{Cu}$  and  $\pi_{azo}^*$  orbitals in  $3^+$ .

$[Cu^{II}(abpy)_2]^{2+}$  ( $3^{2+}$ ). In contrast to the distorted tetrahedral geometry of the  $3^+$  ion, the  $3^{2+}$  ion holds a distorted square planar geometry in which the dihedral angle between two coordinated abpy ligands is  $34^\circ$  only (Chart 2b). The calculated N(7)–N(8) and N(27)–N(28) lengths, 1.255 Å, are similar to those of the  $mer\text{-}1^{2+}$  and  $ctc\text{-}2^{2+}$  ions. In conjunction with the EPR spectral data (Table 7), Mulliken spin density plot as shown in Figure 9c suggests that  $3^{2+}$  ion is a copper(II) complex of type  $[Cu^{II}(abpy)_2]^{2+}$ .

$[Cu^{II}(abpy^{0.5+})(abpy^{0.5-})] \leftrightarrow [Cu^{II}(abpy^{+})(abpy^{-})]$  (**3**). The calculated geometry of **3** is a distorted tetrahedron in which the dihedral angle between two coordinated abpy ligands is  $67^\circ$  (Chart 2c). The azo bond lengths and the spin-density distributions of the optimized geometry of **3** is different from those of the  $3^+$  and  $3^{2+}$  ions. The relatively longer N(7)–N(8) and N(27)–N(28) lengths, 1.305 Å, and the Mulliken spin-density distribution as depicted in Figure 9d of **3** predict the formation of  $abpy^{\bullet-}$  anion radical (significant calculated coupling constants (A): N7, 4.0; N8, 2.1;  $^{13}C3$ , 3.7;  $^{13}C12$ , 4.0; N27, 4.0; N28, 2.1;  $^{13}C23$ , 3.9; and  $^{13}C32$ , 3.9 G following the numbering scheme of  $3^+$  ion as given in Figure 5) coordinated to copper(I) in **3**. The two  $-N=N-$  lengths in

two ligands are same (Table S). Moreover, a significant amount of spin density was detected on the copper ion of **3**. The geometry of  $[Zn(abpy)_2]^+$  was optimized with the doublet spin state with similar basis sets for comparison. In  $[Zn(abpy)_2]^+$  ion, no spin density was detected on the redox innocent zinc(II) ion as illustrated in Figure 9e. The calculated  $-N=N-$  lengths, 1.288 Å, are relatively shorter than those in **3** as summarized in Table S. The relatively longer  $-N=N-$  lengths and spin density on copper ion indicate the oxidation of copper(I) to copper(II) ion synergistically reducing the azo functions of **3**. The ground electronic state of **3** thus has been defined by a hybrid state of  $[Cu^{II}(abpy^{0.5+})(abpy^{0.5-})] \leftrightarrow [Cu^{II}(abpy^{+})(abpy^{-})]$  electronic states.

$[Cu^{II}(abpy^{+})(abpy^{-})]$  ( $3^-$ ). The origin of the irreversible cathodic peak of  $3^+$  ion at  $-0.74$  V as depicted in Figure 12 (see Discussion section) was investigated by optimizing the gas-phase geometry of  $3^-$  ion with singlet spin state. The calculated average  $-N=N-$  bond lengths are 1.337 Å correlating the  $-N=N-$  lengths of the azo anion radical coordinated to the copper(I) ion.<sup>14b,c</sup> The  $3^-$  ion thus is defined by the  $[Cu^{II}(abpy^{+})(abpy^{-})]$  electronic state. As both abpy ligands are reduced by one electron in  $3^-$  ion, the oxidation of copper(I) to copper(II) ion as observed in case of **3** is not noted here. The dihedral angle between two abpy ligands is  $76^\circ$  (Chart 2d) that is similar to that of the copper(I) complex,  $3^+$ ,

but less than that of 3 incorporating a hybrid state of copper(I) and copper(II) ions.

**Spectroelectrochemical Measurements and Time-Dependent DFT Calculations.** The UV–vis–NIR absorption spectra of 3 and  $3^{2+}$  ion in  $\text{CH}_2\text{Cl}_2$  were recorded by the spectroelectrochemical measurements at 298 K, and absorption data are summarized in Table 2. The spectral features during the  $3^+ \rightarrow 3$  and  $3^+ \rightarrow 3^{2+}$  conversions are illustrated in Figure 10a,b. The  $3^+ \rightarrow 3$  conversion proceeds with several isosbestic points in the region of 400–1400 nm and exhibiting a NIR absorption band at 2400–3000 nm as illustrated in the inset of Figure 10a. During the conversion of  $3^+ \rightarrow 3^{2+}$ , the absorption bands of  $3^+$  ion at 806 and 597 nm gradually diminish as depicted in Figure 10b.

The origins of the lower-energy absorption bands of the complexes were elucidated by TD DFT calculations on  $3^+$ , 3, and  $3^{2+}$  ion in  $\text{CH}_2\text{Cl}_2$  using CPCM model. The excitation energies with the oscillator strengths and the transition types are summarized in Supporting Information, Table S1. Analyses of the singlet transitions of  $3^+$  ion asserted that the lower-energy absorption bands at 806 and 597 nm are due to copper(I) to abpy ligand charge transfer, that is, metal-to-ligand charge transfer (MLCT) in nature. The calculated excitation energies of the MLCT transitions of  $3^+$  are 720.56 and 586.8 nm. The  $\lambda_{\text{max}}$  of  $3^+$  at 346 nm (calculated value 369.59 nm) is due to the  $\pi \rightarrow \pi^*$  transition, which is present in *mer*- $1^{2+}$  and *ctc*- $2^{2+}$  ions, respectively, at 346 and 340 nm. In  $3^{2+}$  ion, as copper(I) ion is oxidized to copper(II) ion, the intensity of the MLCT transitions at 806 and 597 nm decreases. However, the absorption feature of 3 (Figure 10a) is different from *mer*- $1^{2+}$ , *ctc*- $2^{2+}$ ,  $3^+$ , and  $3^{2+}$  ions. It displays an NIR band. The NIR absorption band of 3 at 2400–3000 nm is due to the singly occupied  $\pi^*$  ( $\alpha$  highest occupied molecular orbital (HOMO))  $\rightarrow \pi^*$  ( $\alpha$  lowest unoccupied molecular orbital (LUMO)) transition, which is defined as an intervalence ligand-to-ligand charge transfer (IVLLCT). The MLCT bands of  $3^+$  ions at 800 nm shifts to 1049 nm in 3, the origin of which was elucidated as a metal-to-mixed-metal–ligand charge transfer (MMLCT, calculated values 1205.46 and 851.43 nm).

**Reactivities of  $[\text{Cu}(\text{bpy})_3]^{2+}$  and  $[\text{Cu}(\text{phen})_3]^{2+}$  toward Catechol, *o*-Aminophenol, *p*-Phenylenediamine, and Diphenylamine.** To investigate the reactions of *mer*- $1^{2+}$  and  $2^{2+}$  ions toward catechol, *o*-aminophenol, and *p*-phenylenediamine as reduction-induced ligand dissociation or ligand dissociation-induced reduction reactions, we performed the similar reactions of these organic substrates with  $[\text{Cu}(\text{bpy})_3]^{2+}$  and  $[\text{Cu}(\text{phen})_3]^{2+}$ . Note that  $[\text{Cu}(\text{bpy})_3]^{2+}$  and  $[\text{Cu}(\text{phen})_3]^{2+}$  are stable in solution with higher overall stability constants ( $\log(\beta_3) = 17.85$  for  $[\text{Cu}(\text{bpy})_3]^{2+}$  ion).<sup>16c</sup> The reactions were investigated by UV–vis–NIR absorption spectra. The spectral feature during the reaction of  $[\text{Cu}(\text{bpy})_3]^{2+}$  with catechol in  $\text{CH}_2\text{Cl}_2$  is illustrated in Figure 11. The absorption spectral features during the reaction of *o*-aminophenol and *p*-phenylenediamine with  $[\text{Cu}(\text{bpy})_3]^{2+}$  and those with  $[\text{Cu}(\text{phen})_3]^{2+}$  are depicted in Supporting Information, Figure S4.

It is confirmed that in the presence of reducing substrates these tris complexes undergo reduction and ligand dissociation affording  $[\text{Cu}(\text{bpy})_2]^+$  and  $[\text{Cu}(\text{phen})_2]^+$  complexes,<sup>46,47</sup> which summarizes that these redox reactions of these complexes of copper(II) ion are reduction-induced ligand dissociation reaction. The formation of  $[\text{Cu}(\text{bpy})_2]^+$  was followed by the absorption maxima at 434 and 520 nm, and the formation of

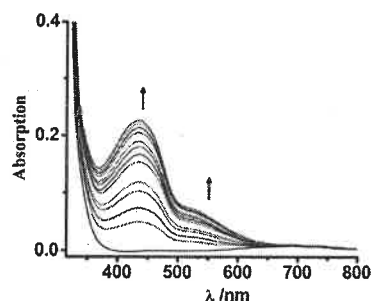
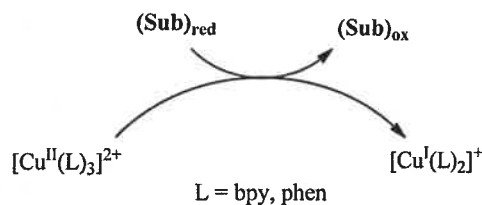


Figure 11. Change of electronic spectra during the reaction of  $[\text{Cu}(\text{bpy})_3]^{2+}$  with catechol in  $\text{CH}_2\text{Cl}_2$  at 298 K.

$[\text{Cu}(\text{phen})_2]^+$  was followed by the absorption maxima at 442 and 528 nm. The isotopic EPR signal in  $\text{CH}_2\text{Cl}_2$  due to octahedral copper(II) ion also gradually diminishes during the reactions of *mer*- $1^{2+}$ , *ctc*- $2^{2+}$ , and  $[\text{Cu}(\text{bpy})_3]^{2+}$  ions with catechol as shown in Supporting Information, Figures S5 and S6, authenticating the formation of copper(I) complexes of abpy, bpy, and phen and the diamagnetic quinone derivatives as depicted in Scheme 3. Formation of the intermediate benzosemiquinone derivative of the organic substrate was not successfully detected.

Scheme 3



## DISCUSSION OF ELECTRONIC STRUCTURES

Octahedral *mer*- $1^{2+}$  and *ctc*- $2^{2+}$  complex ions are oxidizing agents. They react with redox noninnocent organic substrates affording tetrahedral bis(abpy) complex of copper(I) ion,  $3^+$ , as depicted in Scheme 1. Origins of the redox activities were elucidated by the cyclic voltammetry and DFT calculations. It is observed that in *mer*- $1^{2+}$  ion, the  $\beta$ -LUMO is a  $d_z^2$  orbital of copper(II) ion, while the LUMO+1 ( $\alpha$  and  $\beta$ ) are  $\pi_{\text{azo}}^*$  orbital of one of the abpy ligands. The  $\alpha$  and  $\beta$  LUMO+2 and LUMO+3 orbitals are delocalized over the  $\pi_{\text{azo}}^*$  orbitals of the other two equivalent abpy ligands (Supporting Information, Figure S7). Thus, the cathodic wave ( $E_{1/2}^3$ , Table 6) of *mer*- $1^{2+}$  ion at  $-0.42$  V is because of the  $\text{Cu}^{\text{II}}/\text{Cu}^{\text{I}}$  reduction couple. As the copper(I) ion holds a different geometry than that of copper(II) ion, the redox couple is quasi-reversible. Similar redox waves of  $[\text{Cu}(\text{bpy})_3]^{2+}$  and  $[\text{Cu}(\text{phen})_3]^{2+}$  ions due to  $\text{Cu}^{\text{II}}/\text{Cu}^{\text{I}}$  reduction couples at  $+0.04$  and  $+0.03$  V versus saturated calomel electrode (SCE) were reported recently.<sup>16a</sup> However, the current height of the redox wave at  $-0.42$  V of *mer*- $1^{2+}$  is relatively higher compared to those of the reversible redox waves at  $-0.90$  ( $E_{1/2}^3$ , Table 6) and  $-1.28$  V ( $E_{1/2}^4$ , Table 6) because of abpy/abpy $^{\bullet-}$  couples. The cathodic wave of *mer*- $1^{2+}$  ion at  $-0.42$  V was assigned to overlapping  $\text{Cu}^{\text{II}}/\text{Cu}^{\text{I}}$  and abpy/abpy $^{\bullet-}$  (corresponding to localized LUMO+1 orbital) reduction couples. The three redox waves of *mer*- $1^{2+}$  ion at  $-0.42$ ,  $-0.90$ , and  $-1.28$  V because of abpy/abpy $^{\bullet-}$  reduction

couples correlate well to those of the *mer* (−0.49, −0.84, and −1.33 V) and *fac* (−0.41, −0.77, and −1.32 V) isomers of  $[\text{Ru}(\text{abpy})_3]^{2+}$  measured in dimethylformamide.<sup>21</sup> The reduced species of *mer*- $1^{2+}$  ion are not stable in solution and disproportionate to metallic copper, which is detected by the high current at −0.48 V as illustrated in Figure 6a. Expectedly, one of the cathodic waves due to  $\text{abpy}/\text{abpy}^{\bullet-}$  couple is missing in *ctc*- $2^{2+}$  ion. The cathodic wave of *ctc*- $2^{2+}$  ion at −0.44 V ( $E_{1/2}^2$ , Table 6) is assigned to  $\text{Cu}^{2+}/\text{Cu}^+$  couple, while the redox waves at −0.86 ( $E_{1/2}^3$ , Table 6) and −1.10 V ( $E_{1/2}^4$ , Table 6) are assigned to  $\text{abpy}/\text{abpy}^{\bullet-}$  reduction couples. In the experimental scan period, reduced species of *ctc*- $2^{2+}$  ion similar to those of *mer*- $1^{2+}$  ion, deposit metallic copper, which was detected by the higher current at −0.59 V as shown in Figure 6b.

In  $3^+$  ion, two *abpy* ligands are equivalent, and the planes of two *abpy* ligands are approximately orthogonal to each other. The dihedral angle between these two planes is  $80 \pm 1^\circ$  found in both X-ray and optimized geometries as shown in Chart 2. On the contrary,  $3^{2+}$  ion holds a distorted square planar geometry. The calculated dihedral angle between two *abpy* planes is only  $34^\circ$ . Similar distortion of the geometrical features during the conversion of  $[\text{Cu}(\text{bpy})_2]^+$  to  $[\text{Cu}(\text{bpy})_2]^{2+}$  was documented in literature.<sup>45</sup> It was reported that the dihedral angle between the two *bpy* planes is  $84^\circ$  in  $[\text{Cu}^{\text{I}}(\text{bpy})_2]\text{CF}_3\text{SO}_3$ , while the same is only  $38^\circ$  in  $[\text{Cu}^{\text{II}}(\text{bpy})_2](\text{BF}_4)_2$ . The calculated corresponding dihedral angle (gas-phase geometry optimization) in **3** is  $67^\circ$ . These geometrical features of  $3^+$ ,  $3^{2+}$ , and **3** affect significantly the reversibility of the  $3^{2+}/3^+$  and  $3^+/3$  reduction couples (Table 6). Molecular orbital analyses authenticated that the HOMO of  $3^+$  ion is one of the  $t_2$  orbitals, while LUMO and LUMO+1 are delocalized over the  $\pi_{\text{azo}}$  orbitals of the two equivalent *abpy* ligands as depicted in Supporting Information, Figure S8. Thus, the anodic wave of  $3^+$  ion at 0.33 V is assigned to a  $\text{Cu}^{2+}/\text{Cu}^+$  reduction couple, while the cathodic wave at −0.40 V is due to a  $\text{abpy}/\text{abpy}^{\bullet-}$  reduction couple. The similar  $\text{Cu}^{2+}/\text{Cu}^+$  reduction potentials were reported in cases of copper(I) complexes incorporating two redox noninnocent ligands:  $[\text{Cu}^{\text{II}}\text{L}_2]^{2+}/[\text{Cu}^{\text{I}}\text{L}_2]^+$ , where *L* = 2-(phenylazo)pyridine,<sup>48</sup> 0.63 V versus SCE; *L* = 2,9-diphenyl-1,10-phenanthroline (*dpp*),<sup>43b</sup> 0.32 V vs  $\text{Fc}^+/\text{Fc}$ ; *L* = 2,9-dimethyl-1,10-phenanthroline (*dmp*),<sup>43b</sup> 0.30 V versus  $\text{Fc}^+/\text{Fc}$ ; *L* = 2-(arylazo)pyrimidines (*aapm*),<sup>49</sup> 0.63–0.76 V versus SCE; *L* = *N*-aryl-pyridine-2-aldimines,<sup>50</sup> 0.34–0.35 V. The anisotropic EPR spectrum of the  $\text{CH}_2\text{Cl}_2$  frozen glass of  $3^{2+}$  ion (Figure 8a) corroborates with the transformation of copper(I) to copper(II) ion in  $3^{2+}$  ion. The simulated *g* parameters ( $g_1 = 2.105$ ,  $g_2 = 2.228$ ) correlate well to those ( $g_1 = 2.067$ ,  $g_2 = 2.283$ ) reported in case of  $[\text{Cu}^{\text{II}}(\text{dpp})_2]^{2+}$ .<sup>43b</sup> The Mulliken spin density of the doublet  $3^{2+}$  ion is localized on the copper ion (Figure 9b), and the  $3^{2+}$  ion is defined as a copper(II) complex of *abpy* ligands of type  $[\text{Cu}^{\text{II}}(\text{abpy})_2]^{2+}$ .

On the basis of the constituents of the LUMO and LUMO+1 orbitals, the reversible cathodic wave of  $3^+$  ion at −0.40 V is assigned to a  $\text{abpy}/\text{abpy}^{\bullet-}$  reduction couple. Solid ( $g = 2.001$ ), fluid solution ( $g = 2.001$ ,  $A_{\text{N}} = 14$  G), and frozen glass ( $g_1 = g_2 = 1.999$ ,  $A_{1(\text{N})} = 8$  and  $A_{2(\text{N})} = 16$  G) EPR spectra and the DFT calculation (vide supra) support the proposition of the coordination of  $\text{abpy}^{\bullet-}$  anion radical to the copper(I) ion in **3**. Note that the potentials of the cathodic waves of  $[\text{Cu}^{\text{I}}(\text{L})_2]^+$  types of complexes depend significantly on the  $\pi$ -acidity of *L*, which implies that these redox waves are generally because of the  $\text{L}/\text{L}^{\bullet-}$  reduction couple. The claim of the formations of bis[2,9-di(*o*-substituted phenyl)-1,10-phenanthroline]copper(0)

complexes upon reduction of bis[2,9-di(*o*-substituted phenyl)-1,10-phenanthroline]copper(I) had never been justified by the EPR spectra.<sup>51</sup> Kaim et al. after rigorous electrochemical studies substantiated that the reduction occurs at the phenanthroline ligand fragments. The  $\text{dpp}/\text{dpp}^{\bullet-}$  and  $\text{dmp}/\text{dmp}^{\bullet-}$  reduction couples in  $[\text{Cu}^{\text{I}}(\text{dpp})_2]^+$  and  $[\text{Cu}^{\text{I}}(\text{dmp})_2]^+$  were observed at −2.02 and −2.13 V versus  $\text{Fc}^+/\text{Fc}$ .<sup>43b</sup> In the cases of azopyrimidine derivatives, the *aapm*/*aapm* $^{\bullet-}$  reduction couples in  $[\text{Cu}^{\text{I}}(\text{aapm})_2]^+$  complexes were recorded at −0.63 to −0.76 V versus SCE.<sup>49</sup> As the *abpy* is a stronger  $\pi$  acidic N,N-donor ligand, the  $\text{abpy}/\text{abpy}^{\bullet-}$  reduction potential in **3** shifts to −0.40 V (Table 6), and it is the lowest reduction potential reported so far for the  $[\text{CuL}_2]^+$  types of complexes. However, the reduced species are not stable in solution. Scanning at higher potentials even within the experimental time scale, the reduced complexes disproportionate depositing metallic copper that is detected by the higher current at −0.32 V as given in Figure 12. However, the reduction of *abpy* to  $\text{abpy}^{\bullet-}$  radical in **3** was authenticated by the EPR spectra and the DFT calculations.

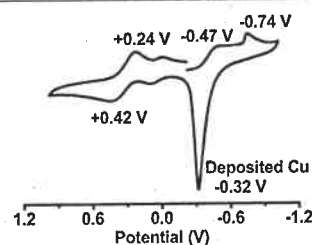
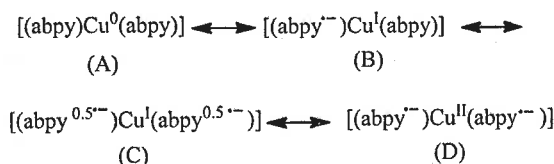


Figure 12. Cyclic voltammogram (+1.0 to −1.0 V vs  $\text{Fc}^+/\text{Fc}$ ) of  $3^+[\text{PF}_6]^-$  in  $\text{CH}_2\text{Cl}_2$  and  $\text{CH}_3\text{CN}$  (5:1) mixture at 298 K. Conditions: 0.2 M  $[\text{N}(\text{n-Bu})_4]\text{PF}_6$  supporting electrolyte; scan rate, 100  $\text{mV s}^{-1}$ ; platinum working electrode.

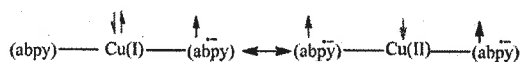
The hyperfine spectra due to coupling of azo  $^{14}\text{N}$  nuclei were detected in cases of fluid solution and frozen glass EPR spectra of **3** as shown in Figure 8c,d. The simulated coupling constant values of the frozen glass are  $A_{1(\text{N})} = 8$  and  $A_{2(\text{N})} = 16$  G (Table 7). Calculated significant coupling constant values due to azo N and other atoms are listed in DFT Calculation Section of 3. The Mulliken spin density is delocalized over *abpy* ligands. As the LUMO is equally distributed over the two  $\pi_{\text{azo}}$  orbitals, the fractional negative charges scatter equally over the two equivalent *abpy* ligands as observed in the spin-density plot as illustrated in Figure 9d. Two calculated azo lengths are same informing that the extent of reduction of the two ligands is same. The feature is similar to that of  $[\text{Ni}^{\text{II}}(\text{R}^{\text{L}}\text{O}_2^{\bullet-})_2]^+$ , a Robin–Day class III species, where the radical spin is equally delocalized over two equivalent deprotonated  $\beta$ -diketiminato ligands ( $\text{R}^{\text{L}}^-$ ) and coupled to  $S = 1$  state of Ni(II) ion furnishing an  $S_{\text{t}} = 1/2$  state, reported recently.<sup>44</sup> Thus, the electronic state of **3** is defined by the state (C) rather than states (A) and (B) of Scheme 4.

#### Scheme 4



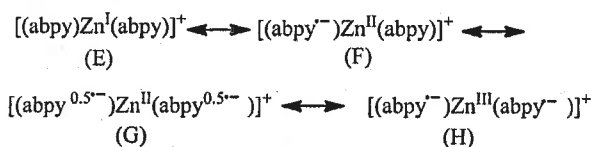
In case of **3**, the localization of significant opposite spin ( $\beta$  spin) on copper ion to that of abpy ligand, as depicted in Figure 9d, compelled us to investigate further to elucidate the ground electronic state of **3** correctly. The spin density on copper ion in **3** is defined as a reduction-induced oxidation of Cu(I) to Cu(II) ion affording the electronic state,  $[\text{Cu}^{\text{II}}(\text{abpy}^{\bullet-})-(\text{abpy}^{\bullet-})]$ , (**D**) of Scheme 3. The driving force of this reduction-induced oxidation of copper(I) to copper(II) ion in **3** is the higher exchange energy due to coupling of the unpaired electrons of the copper ion and  $\text{abpy}^{\bullet-}$  anion radical. The coupling constant ( $J$ ) was calculated using Yamaguchi approach.<sup>39</sup> The  $J_{\text{cal}}$  is  $-2170 \text{ cm}^{-1}$ , and the coupling scheme is  $\uparrow\text{Cu}\downarrow\text{L}\uparrow$ , which is achieved by an electron transfer from copper(I) to an abpy ligand, as depicted in Chart 3. The amount of  $\beta$  spin localized on copper ion and the coordination sites is ca.  $-0.50$ , which predicts a reasonable contribution of state **D** to the electronic state of **3**.

Chart 3



The coupling scheme is different from that of a transition metal complex with two planar  $\pi$  radical ligands.<sup>52</sup> However, the similar coupling scheme of copper(II) ion incorporating two nonplanar iminobenzosemiquinone radicals was reported recently by Kaim et al.<sup>53</sup> The analogy of higher coupling energy induced oxidation of copper(I) to copper(II) ion was substantiated by optimizing the  $[\text{Zn}(\text{abpy})_2]^+$  cation (with doublet spin state), which is isoelectronic to **3**. The calculated bond parameters are listed in Table S, and the Mulliken spin-density plot is shown in Figure 9e. Similar to **3**, two abpy ligands are equally reduced, implying the existence of the electronic state (**G**) of Scheme 5 in  $[\text{Zn}(\text{abpy})_2]^+$  ion.

Scheme 5



Expectedly, no spin density is localized on the zinc ion forbidding the electronic state (**H**) to contribute to the ground electronic state of  $[\text{Zn}(\text{abpy})_2]^+$  ion. It correlates well to the relatively shorter  $-\text{N}=\text{N}-$  lengths in  $[\text{Zn}(\text{abpy})_2]^+$  ion compared to those of **3**. The extent of reduction of azo functions of **3** is relatively higher due to easy oxidation of copper(I) to copper(II) ion in **3**.

Thus, the ground electronic state of  $[\text{Zn}(\text{abpy})_2]^+$  ion is defined by the electronic state  $[\text{Zn}^{\text{II}}(\text{abpy}^{0.5\bullet-})(\text{abpy}^{0.5\bullet-})]$  (**G**) of Scheme 5, while that of **3** is defined by a hybrid state of the electronic states,  $[\text{Cu}^{\text{I}}(\text{abpy}^{0.5\bullet-})(\text{abpy}^{0.5\bullet-})] \leftrightarrow [\text{Cu}^{\text{II}}(\text{abpy}^{\bullet-})(\text{abpy}^{\bullet-})]$ , (**C**) and (**D**) of Scheme 4. The existence of two reduced ligands is further correlated by the IVLLCT absorption band of **3** at 2400–3000 nm as depicted in Figure 10. The contribution of copper(II) ion to the ground electronic state of **3** is also supported by the dihedral angle ( $\varphi$ ) between two abpy ligands as given in Chart 2. The least  $\varphi$  is  $34^\circ$  for  $3^{2+}$  ion, which is a copper(II) complex of type  $[\text{Cu}^{\text{II}}(\text{abpy})_2]^{2+}$ , while it is  $81^\circ$  for  $3^+$  ion, which is a copper(I) complex of type  $[\text{Cu}^{\text{I}}(\text{abpy})_2]^+$ .

In **3**, the  $\varphi$  is  $67^\circ$  being an intermediate value of those of  $3^{2+}$  and  $3^+$  ions. Surprisingly the calculated  $\varphi$  ( $76^\circ$ ) is relatively higher in  $[\text{Cu}^{\text{I}}(\text{abpy}^{\bullet-})(\text{abpy}^{\bullet-})]^-$  (**3**<sup>−</sup>) ion where both the abpy ligands are reduced by one electron forbidding the deformation of geometry due to conversion of copper(I) to copper(II) ion as observed in case of **3**.

## CONCLUSION

2,2'-Azobispyridine (abpy) is a bidentate N,N-donor redox noninnocent ligand that developed a rich azo anion radical chemistry with transition metal ions. However, tris(abpy) complexes are rare, and the only isolated complex of this type was  $[\text{Ru}^{\text{II}}(\text{abpy})_3]^{2+}$ , which is not characterized crystallographically yet. In this article, we report on *mer*- $[\text{Cu}^{\text{II}}(\text{abpy})_3]^{2+}$  (*mer*-**1**<sup>2+</sup>) and *ctc*- $[\text{Cu}^{\text{II}}(\text{abpy})_2(\text{bpy})]^{2+}$  (*ctc*-**2**<sup>2+</sup>) complexes. The single-crystal X-ray bond parameters of *mer*-**1**<sup>2+</sup> $[\text{PF}_6^-]$  and *ctc*-**2**<sup>2+</sup> $[\text{PF}_6^-]$  are significant to analyze the direction of Jahn–Teller distortion. It is disclosed that *mer*-**1**<sup>2+</sup> and *ctc*-**2**<sup>2+</sup> ions and the similar analogues of bpy and phen of types  $[\text{Cu}^{\text{II}}(\text{bpy})_3]^{2+}$  and  $[\text{Cu}^{\text{II}}(\text{phen})_3]^{2+}$  ions react with redox noninnocent organic substrates like catechol, *o*-aminophenol, diphenylamine (Ph–NH–Ph), and *p*-phenylenediamine affording  $[\text{Cu}^{\text{I}}(\text{abpy})_2]^+$ ,  $[\text{Cu}^{\text{I}}(\text{bpy})_2]^+$ , and  $[\text{Cu}^{\text{I}}(\text{phen})_2]^+$  ions and corresponding two-electron oxidized quinone products. These conversions are defined as reduction-induced ligand dissociation reactions. These redox reactions compare well to those reactions catalyzed by catecholoxidase<sup>22</sup> and aminophenoloxidase.<sup>23</sup> It has been established that  $3^{2+}$  ion converts to  $2^{2+}$  ion in the presence of excess bpy, which suggests that the reduction-induced ligand dissociation reactions of *mer*-**1**<sup>2+</sup> and *ctc*-**2**<sup>2+</sup> ions and vice versa as shown in Scheme 2 are reversible in nature.

The  $3^+$  ion, which is a neutral abpy (average experimental  $-\text{N}=\text{N}-$  lengths, 1.275(2) Å) complex of copper(I) ion, is redox-active, and both anodic and cathodic waves at +0.33 and −0.40 V because of  $\text{Cu}^{2+}/\text{Cu}^+$  and  $\text{abpy}/\text{abpy}^{\bullet-}$  reduction couples are reversible. The ground electronic structures of electrogenerated  $3^{2+}$  and **3** were substantiated by spectroelectrochemical measurements, EPR spectra, DFT, and TD DFT calculations. The simulated  $g$  values ( $2.000 \pm 0.001$ ) of the solid, fluid solution, and frozen glass EPR spectra authenticated that  $3^+ \rightarrow 3$  conversion is due to the formation of delocalized  $\text{abpy}^{\bullet-}$  anion radicals (average calculated  $-\text{N}=\text{N}-$  lengths, 1.305 Å) coordinated to copper(I) ion. However, localization of significant Mulliken spin densities on the metal ion suggests the oxidation of copper(I) ion to copper(II) ion that promotes higher coupling exchange energy ( $J_{\text{cal}} = -2170 \text{ cm}^{-1}$ ) following a coupling scheme of type  $\uparrow\text{Cu}\downarrow\text{L}\uparrow$ . Thus, the ground electronic state of **3** is defined as a hybrid state of  $[\text{Cu}^{\text{I}}(\text{abpy}^{0.5\bullet-})(\text{abpy}^{0.5\bullet-})]$  and  $[\text{Cu}^{\text{II}}(\text{abpy}^{\bullet-})(\text{abpy}^{\bullet-})]$  states. **3** being a Robin–Day class III species, exhibits NIR absorption band at 2400–3000 nm due to the IVLLCT. Frozen glass EPR spectral parameters ( $g_1$ , 2.105 and  $g_2$ , 2.228) and the Mulliken spin density distribution authenticated that  $3^{2+}$  is a copper(II) complex of neutral abpy ligand (average calculated  $-\text{N}=\text{N}-$  lengths, 1.255 Å) of type  $[\text{Cu}^{\text{II}}(\text{abpy})_2]^{2+}$ .

## ASSOCIATED CONTENT

### Supporting Information

X-ray crystallographic CIF files for the *mer*-**1**<sup>2+</sup> $[\text{PF}_6^-]_2$ , *ctc*-**2**<sup>2+</sup> $[\text{PF}_6^-]_2$ , and **3**<sup>+</sup> $[\text{PF}_6^-]$  complexes; change of electronic spectra of *mer*-**1**<sup>2+</sup> $[\text{PF}_6^-]_2$  and *ctc*-**2**<sup>2+</sup> $[\text{PF}_6^-]$  upon addition of *p*-phenylenediamine, *o*-aminophenol, catechol, and diphenyl-

amine; cyclic voltammograms of  $\text{mer-1}^{2+}[\text{PF}_6^-]_2$  in  $\text{CH}_2\text{Cl}_2/\text{CH}_3\text{CN}$  (5:1) solvents in multiple scan rates; gas-phase optimized geometries of  $\text{mer-1}^{2+}$ ,  $\text{ctc-2}^{2+}$ ,  $3^+$ ,  $3$ , and  $3^{2+}$ ; excitation energies, oscillator strengths, transition types, and dominant contributions to UV-vis-NIR absorption spectra of  $3^+$ ,  $3$ , and  $3^{2+}$  obtained from TD DFT calculations; change of electronic spectra of  $[\text{Cu}(\text{bpy})_3]^{2+}$  and  $[\text{Cu}(\text{phen})_3]^{2+}$  during the reactions with catechol, *p*-phenylenediamine, and *o*-aminophenol; change of EPR spectra during the transformations of (a)  $1^{2+} \rightarrow 3^+$  and (b)  $2^{2+} \rightarrow 3^+$  in the presence of catechol in  $\text{CH}_2\text{Cl}_2$  at 273 K; change of EPR spectra during the transformation of  $[\text{Cu}(\text{bpy})_3]^{2+} \rightarrow [\text{Cu}(\text{bpy})_2]^+$  in the presence of catechol in  $\text{CH}_2\text{Cl}_2$  at 273 K; frontier orbitals of  $1^{2+}$ ,  $3^+$ ,  $3^{2+}$ , and  $3$ ; optimized coordinates of  $\text{mer-1}^{2+}$ ,  $\text{ctc-2}^{2+}$ ,  $3^+$ ,  $3^{2+}$ ,  $3$ ,  $3^+$ , and  $[\text{Zn}(\text{abpy})_2]^+$ . This material is available free of charge via the Internet at <http://pubs.acs.org>.

## AUTHOR INFORMATION

### Corresponding Author

\*E-mail: [ghosh@pghosh.in](mailto:ghosh@pghosh.in). Phone: +91-33-2428-7347. Fax: +91-33-2477-3597.

### Author Contributions

The manuscript was written through contributions of all authors. All authors have given approval to the final version of the manuscript.

### Notes

The authors declare no competing financial interest.

## ACKNOWLEDGMENTS

Financial support received from DST (SR/S1/IC/0026/2012) and CSIR 01(2699/12/EMR-II) New Delhi, India, is gratefully acknowledged. S.M. and S.K. are thankful to CSIR, New Delhi, India, for fellowships.

## REFERENCES

- (1) (a) Kim, E.; Chufan, E. E.; Kamaraj, K.; Karlin, K. D. *Chem. Rev.* 2004, 104, 1077–1133. (b) Ferguson-Miller, S. *Chem. Rev.* 1996, 96, 2889–2907.
- (2) (a) Saito, T.; Thiel, W. J. *Phys. Chem. B* 2014, 118, 5034–5043. (b) Magnus, K. A.; Ton-That, H.; Carpenter, J. E. *Chem. Rev.* 2004, 94, 727–735.
- (3) Solomon, E. I.; Heppner, D. E.; Johnston, E. M.; Ginsbach, J. W.; Cirera, J.; Qayyum, M.; Kieber-Emmons, M. T.; Kjaergaard, C. H.; Hadt, R. G.; Tian, L. *Chem. Rev.* 2014, 114, 3659–3853.
- (4) Winkler, J. R.; Gray, H. B. *Chem. Rev.* 2014, 114, 3369–3380.
- (5) Boal, A. K.; Rosenzweig, A. C. *Chem. Rev.* 2009, 109, 4760–4779.
- (6) Rorabacher, D. B. *Chem. Rev.* 2004, 104, 651–697.
- (7) Solomon, E. I.; Szilagyi, R. K.; George, S. D.; Basumallick, L. *Chem. Rev.* 2004, 104, 419–458.
- (8) (a) Halvagar, M. R.; Solntsev, P. V.; Lim, H.; Hedman, B.; Hodgson, K. O.; Solomon, E. I.; Cramer, C. J.; Tolman, W. B. *J. Am. Chem. Soc.* 2014, 136, 7269–7272. (b) Barnett, S. M.; Goldberg, K. I.; Mayer, J. M. *Nat. Chem.* 2012, 4, 498–502. (c) Donoghue, P. J.; Gupta, A. K.; Boyce, D. W.; Cramer, C. J.; Tolman, W. B. *J. Am. Chem. Soc.* 2010, 132, 15869–15871. (d) Halfen, J. A.; Fox, D. C.; Mehn, M. P.; Que, J. L. *Inorg. Chem.* 2001, 40, 5060–5061. (e) Chaudhuri, P.; Hess, M.; Müller, J.; Hildenbrand, K.; Bill, E.; Weyhermüller, T.; Wieghardt, K. *J. Am. Chem. Soc.* 1999, 121, 9599–9610. (f) Wang, Y.; DuBois, J. L.; Hedman, B.; Hodgson, K. O.; Stack, T. D. P. *Science* 1998, 279, 537–540.
- (9) Allen, S. E.; Walvoord, R. R.; Padilla-Salinas, R.; Kozłowski, M. C. *Chem. Rev.* 2013, 113, 6234–6458.
- (10) (a) Citec, C.; Lyons, C. T.; Wasinger, E. C.; Stack, T. D. P. *Nat. Chem.* 2012, 4, 317–322. (b) Hong, S.; Gupta, A. K.; Tolman, W. B. *Inorg. Chem.* 2009, 48, 6323–6325. (c) Jiang, D.; Men, L.; Wang, J.;

- Zhang, Y.; Chickenyen, S.; Wang, Y.; Zhou, F. *Biochemistry* 2007, 46, 9270–9282. (d) Lewis, E. A.; Tolman, W. B. *Chem. Rev.* 2004, 104, 1047–1076.
- (11) (a) Gupta, A. K.; Tolman, W. B. *Inorg. Chem.* 2012, 51, 1881–1888. (b) Canary, J. W.; Mortezaei, S.; Liang, J. *Chem. Commun.* 2010, 46, 5850–5860. (c) Osako, T.; Tachi, Y.; Taki, M.; Fukuzumi, S.; Itoh, S. *Inorg. Chem.* 2001, 40, 6604–6609. (d) Balamurugan, R.; Palaniandavar, M. *Inorg. Chem.* 2001, 40, 2246–2255. (e) Ambundo, E. A.; Deydier, M.-V.; Grall, A. J.; Agüera-Vega, N.; Dressel, L. T.; Cooper, T. H.; Heeg, M. J.; Ochrymowycz, L. A.; Rorabacher, D. B. *Inorg. Chem.* 1999, 38, 4233–4242.
- (12) (a) Patra, S. C.; Weyhermüller, T.; Ghosh, P. *Inorg. Chem.* 2014, 53, 2427–2440. (b) McKinnon, S. D. J.; Patrick, B. O.; Lever, A. B. P.; Hicks, R. G. *Inorg. Chem.* 2013, 52, 8053–8066. (c) Kundu, S.; Maity, S.; Weyhermüller, T.; Ghosh, P. *Inorg. Chem.* 2013, 52, 7417–7430. (d) Shaffer, D. W.; Szigethy, G.; Ziller, J. W.; Heyduk, A. F. *Inorg. Chem.* 2013, 52, 2110–2118. (e) Szigethy, G.; Shaffer, D. W.; Heyduk, A. F. *Inorg. Chem.* 2012, 51, 12606–12618. (f) Chirik, P. J. *Inorg. Chem.* 2011, 50, 9737–9740. (g) Kaim, W. *Inorg. Chem.* 2011, 50, 9752–9765. (h) Pierpont, C. G. *Inorg. Chem.* 2011, 50, 9766–9772. (i) Dzik, W. I.; Zhang, X. P.; de Bruin, B. *Inorg. Chem.* 2011, 50, 9896–9903. (j) Lippert, C. A.; Hardcastle, K. I.; Soper, J. D. *Inorg. Chem.* 2011, 50, 9864–9878. (k) Das, D.; Sarkar, B.; Mondal, T. K.; Mobin, S. M.; Fiedler, J.; Kaim, W.; Lahiri, G. K. *Inorg. Chem.* 2011, 50, 7090–7098. (l) Cowley, R. E.; Bill, E.; Neese, F.; Brennessel, W. W.; Holland, P. L. *Inorg. Chem.* 2009, 48, 4828–4836. (m) Nguyen, A. I.; Blackmore, K. J.; Carter, S. M.; Zarkesh, R. A.; Heyduk, A. F. *J. Am. Chem. Soc.* 2009, 131, 3307–3316. (n) Kapre, R. R.; Bothe, E.; Weyhermüller, T.; George, S. D.; Muresan, N.; Wieghardt, K. *Inorg. Chem.* 2007, 46, 7827–7839. (o) Kaim, W.; Lahiri, G. K. *Angew. Chem., Int. Ed.* 2007, 46, 1778–1796. (p) Barclay, T. M.; Hicks, R. G.; Lemaire, M. T.; Thompson, L. K. *Inorg. Chem.* 2001, 40, 6521–6524. (q) Barclay, T. M.; Hicks, R. G.; Lemaire, M. T.; Thompson, L. K. *Inorg. Chem.* 2001, 40, 5581–5584.
- (13) (a) Baldwin, D. A.; Lever, A. B. P.; Parish, R. V. *Inorg. Chem.* 1969, 8, 107–115. (b) Kirpal, A.; Reiter, L. *Ber. Dtsch. Chem. Ges.* 1927, 60, 664–666.
- (14) (a) Sarkar, B.; Patra, S.; Fiedler, J.; Sunoj, R. B.; Janardanan, D.; Lahiri, G. K.; Kaim, W. *J. Am. Chem. Soc.* 2008, 130, 3532–3542. (b) Kaim, W. *Dalton Trans.* 2003, 5, 761–768. (c) Doslik, N.; Sixt, T.; Kaim, W. *Angew. Chem., Int. Ed.* 1998, 37, 2403–2404. (d) Frantz, S.; Hartmann, H.; Doslik, N.; Wanner, M.; Kaim, W.; Kümmerer, H.-J.; Denninger, G.; Barra, A.-L.; Duboc-Toia, C.; Fiedler, J.; Ciofini, I.; Urban, C.; Kaupp, M. *J. Am. Chem. Soc.* 1990, 112, 173–178.
- (15) (a) Bertini, I.; Dapporto, P.; Gatteschi, D.; Scozzafava, A. J. *Chem. Soc., Dalton Trans.* 1979, 1409–1414. (b) Cullen, D. L.; Lingafelter, E. C. *Inorg. Chem.* 1970, 9, 1858–1864.
- (16) (a) Majumdar, P.; Ghosh, A. K.; Falvello, L. R.; Peng, S.-M.; Goswami, S. *Inorg. Chem.* 1998, 37, 1651–1654. (b) Anderson, O. P. *J. Chem. Soc., Dalton Trans.* 1972, 2597–2601. (c) Onstott, E. I.; Laitinen, H. A. *J. Am. Chem. Soc.* 1950, 72, 4724–4728.
- (17) (a) Oh, M.-J.; Lee, Y.-M.; Lee, S. J.; Kang, S. K.; Choi, S.-N. *Acta Crystallogr.* 2006, C62, m51–m53. (b) Garmendia, G.; Quiros, M. J. *Coord. Chem.* 2002, 3, 345–351.
- (18) (a) Das, A.; Scherer, T. M.; Chowdhury, A. D.; Mobin, S. M.; Kaim, W.; Lahiri, G. K. *Inorg. Chem.* 2012, 51, 1675–1684. (b) Sarkar, B.; Patra, S.; Fiedler, J.; Sunoj, R. B.; Janardanan, D.; Mobin, S. M.; Niemeyer, M.; Lahiri, G. K.; Kaim, W. *Angew. Chem., Int. Ed.* 2005, 44, 5655–5658. (c) Campos-Fernandez, C. S.; Galán-Mascarós, J. R.; Smucker, B. W.; Dunbar, K. R. *Eur. J. Inorg. Chem.* 2003, 5, 988–994. (d) Kaim, W. *Coord. Chem. Rev.* 2001, 219–221, 463–488. (e) Kaim, W.; Kohlmann, S.; Jordanov, J.; Fenske, D. *Z. Anorg. Allg. Chem.* 1991, 598–599, 217–234. (f) Baldwin, D. A.; Lever, A. B. P.; Parish, R. V. *Inorg. Chem.* 1969, 8, 107–115.
- (19) (a) Wang, M.; England, J.; Weyhermüller, T.; Wieghardt, K. *Inorg. Chem.* 2014, 53, 2276–2287. (b) England, J.; Wieghardt, K. *Inorg. Chem.* 2013, 52, 10067–10079. (c) Gerasimova, T. P.; Katsyuba, S. A. *Dalton Trans.* 2013, 42, 1787–1797. (d) Lalevée, J.; Blanchard, N.; Tehfe, M. A.; Morlet-Savary, F.; Fouassier, J. P. *Macromolecules*



- 2010, 43, 10191–10195. (e) Liu, W.; Xu, W.; Lin, J.-L.; Xie, H.-Z. *Acta Crystallogr.* 2008, E64, m1586. (f) Zhou, G.; Harruna, I. I. *Macromolecules* 2004, 37, 7132–7139. (g) Fletcher, N. C.; Nieuwenhuyzen, M.; Rainey, S. J. *Chem. Soc., Dalton Trans.* 2001, 2641–2648. (h) Hernández-Molina, M.; Lloret, F.; Ruiz-Pérez, C.; Julve, M. *Inorg. Chem.* 1998, 37, 4131–4135.
- (20) (a) Samanta, S.; Ghosh, P.; Goswami, S. *Dalton Trans.* 2012, 41, 2213–2226. (b) Hotze, A. C. G.; van der Geer, E. P. L.; Kooijman, H.; Spek, A. L.; Haasnoot, J. G.; Reedijk, J. *Eur. J. Inorg. Chem.* 2005, 13, 2648–2657. (c) Ackermann, M. N.; Kühne, S. R.; Saunders, P. A.; Barnes, C. E.; Stallings, S. C.; Kim, H.; Woods, C.; Lagunoff, M. *Inorg. Chim. Acta* 2002, 334, 193–201. (d) Kharmawphlang, W.; Choudhury, S.; Deb, A. K.; Goswami, S. *Inorg. Chem.* 1995, 34, 3826–3828. (e) Ackermann, M. N.; Barton, C. R.; Deodene, C. J.; Specht, E. M.; Keill, S. C.; Schreiber, W. E.; Kim, H. *Inorg. Chem.* 1989, 28, 397–403. (f) Krejčík, M.; Zalis, S.; Klima, J.; Sykora, D.; Matheis, W.; Klein, A.; Kaim, W. *Inorg. Chem.* 1993, 32, 3362–3368.
- (22) (a) Rolff, M.; Schottenheim, J.; Decker, H.; Tuczek, F. *Chem. Soc. Rev.* 2011, 40, 4077–4098. (b) Decker, H.; Schweikardt, T.; Tuczek, F. *Angew. Chem., Int. Ed.* 2006, 45, 4546–4550. (c) Matoba, Y.; Kumagai, T.; Yamamoto, A.; Yoshitsu, H.; Sugiyama, M. *J. Biol. Chem.* 2006, 281, 8981–8990. (d) Senior, S. Z.; Mans, L. L.; VanGuilder, H. D.; Kelly, K. A.; Hendrich, M. P.; Elgren, T. E. *Biochemistry* 2003, 42, 4392–4397. (e) Klabunde, T.; Eicken, C.; Sacchettini, J. C.; Krebs, B. *Nat. Struct. Biol.* 1998, 5, 1084–1090. (f) Tremolieres, M.; Bieth, J. B. *Phytochemistry* 1984, 23, 501–505.
- (23) Nair, P. M.; Vaidynathan, C. S. *Biochim. Biophys. Acta* 1964, 81, 507–516.
- (24) (a) Chang, C. M.; Klema, V. J.; Johnson, B. J.; Mure, M.; Klinman, J. P.; Wilmot, C. M. *Biochemistry* 2010, 49, 2540–2550. (b) Murray, J. M.; Convery, M. A.; Phillips, S. E.; McPherson, M. J.; Knowles, P. F.; Parsons, M. R.; Wilmot, C. M.; Blakeley, V.; Corner, A. S.; Alton, G.; Palcic, M. M. *Biochemistry* 1997, 36, 1608–1620. (c) Tanizawa, K.; Guss, J. M.; Freeman, H. C.; Yamaguchi, H.; Wilce, M. C.; Dooley, D. M.; Matsunami, H.; McIntire, W. S.; Ruggiero, C. E. *Biochemistry* 1997, 36, 16116–16133. (d) Convery, M. A.; Phillips, S. E.; McPherson, M. J.; Yadav, K. D.; Knowles, P. F.; Parsons, M. R.; Wilmot, C. M.; Blakeley, V.; Corner, A. S. *Structure* 1995, 3, 1171–1184.
- (25) Boltz, M.; Blanc, A.; Laugel, G.; Pale, P.; Louis, B. *Chin. J. Catal.* 2011, 32, 807–811.
- (26) Sheldrick, G. M. *ShelXS97*; Universität Göttingen: Göttingen, Germany, 1997.
- (27) Sheldrick, G. M. *ShelXL97*; Universität Göttingen: Göttingen, Germany, 1997.
- (28) Frisch, M. J.; Trucks, G. W.; Schlegel, H. B.; Scuseria, G. E.; Robb, M. A.; Cheeseman, J. R.; Montgomery, J. A., Jr.; Vreven, T.; Kudin, K. N.; Burant, J. C.; Millam, J. M.; Iyengar, S. S.; Tomasi, J.; Barone, V.; Mennucci, B.; Cossi, M.; Scalmani, G.; Rega, N.; Petersson, G. A.; Nakatsuji, H.; Hada, M.; Ehara, M.; Toyota, K.; Fukuda, R.; Hasegawa, J.; Ishida, M.; Nakajima, T.; Honda, Y.; Kitao, O.; Nakai, H.; Klene, M.; Li, X.; Knox, J. E.; Hratchian, H. P.; Cross, J. B.; Bakken, V.; Adamo, C.; Jaramillo, J.; Gomperts, R.; Stratmann, R. E.; Yazyev, O.; Austin, A. J.; Cammi, R.; Pomelli, C.; Ochterski, J. W.; Ayala, P. Y.; Morokuma, K.; Voth, G. A.; Salvador, P.; Dannenberg, J. J.; Zakrzewski, V. G.; Dapprich, S.; Daniels, A. D.; Strain, M. C.; Farkas, O.; Malick, D. K.; Rabuck, A. D.; Raghavachari, K.; Foresman, J. B.; Ortiz, J. V.; Cui, Q.; Baboul, A. G.; Clifford, S.; Cioslowski, J.; Stefanov, B. B.; Liu, G.; Liashenko, A.; Piskorz, P.; Komaromi, I.; Martin, R. L.; Fox, D. J.; Keith, T.; Al-Laham, M. A.; Peng, C. Y.; Nanayakkara, A.; Challacombe, M.; Gill, P. M. W.; Johnson, B.; Chen, W.; Wong, M. W.; Gonzalez, C.; Pople, J. A. *Gaussian 03*, Revision E.01; Gaussian, Inc.: Wallingford, CT, 2004.
- (29) (a) Parr, R. G.; Yang, W. *Density Functional Theory of Atoms and Molecules*; Oxford University Press: Oxford, U.K., 1989. (b) Salahub, D. R.; Zerner, M. C. *The Challenge of d and f Electrons*; ACS Symposium Series 394; American Chemical Society: Washington, DC, 1989. (c) Kohn, W.; Sham, L. J. *J. Phys. Rev.* 1965, 140, A1133–A1138. (d) Hohenberg, P.; Kohn, W. *Phys. Rev.* 1964, 136, B864–B871.
- (30) (a) Stratmann, R. E.; Scuseria, G. E.; Frisch, M. J. *Chem. Phys.* 1998, 109, 8218–8224. (b) Casida, M. E.; Jamorowski, C.; Casida, K. C.; Salahub, D. R. *J. Chem. Phys.* 1998, 108, 4439–4449. (c) Bauernschmitt, R.; Haser, M.; Treutler, O.; Ahlrichs, R. *Chem. Phys. Lett.* 1996, 256, 454–464.
- (31) (a) Becke, A. D. *J. Chem. Phys.* 1993, 98, 5648–5652. (b) Miehlich, B.; Savin, A.; Stoll, H.; Preuss, H. *Chem. Phys. Lett.* 1989, 157, 200–206. (c) Lee, C.; Yang, W.; Parr, R. G. *Phys. Rev. B* 1988, 37, 785–789.
- (32) Pulay, P. *J. Comput. Chem.* 1982, 3, 556–560.
- (33) Schlegel, H. B.; McDouall, J. J. In *Computational Advances in Organic Chemistry*; Ogretir, C., Csizmadia, I. G., Eds.; Kluwer Academic: The Netherlands, 1991.
- (34) (a) Hay, P. J.; Wadt, W. R. *J. Chem. Phys.* 1985, 82, 270–283. (b) Wadt, W. R.; Hay, P. J. *J. Chem. Phys.* 1985, 82, 284–298. (c) Hay, P. J.; Wadt, W. R. *J. Chem. Phys.* 1985, 82, 299–310.
- (35) (a) Rassolov, V. A.; Ratner, M. A.; Pople, J. A.; Redfern, P. C.; Curtiss, L. A. *J. Comput. Chem.* 2001, 22, 976–984. (b) Franch, M. M.; Pietro, W. J.; Hehre, W. J.; Binkley, J. S.; DeFrees, D. J.; Pople, J. A.; Gordon, M. S. *J. Chem. Phys.* 1982, 77, 3654–3665. (c) Hariharan, P. C.; Pople, J. A. *Mol. Phys.* 1974, 27, 209–214. (d) Hariharan, P. C.; Pople, J. A. *Theor. Chim. Acta* 1973, 28, 213–222. (e) Hehre, W. J.; Ditchfield, R.; Pople, J. A. *J. Chem. Phys.* 1972, 56, 2257–2261.
- (36) Hehre, W. J.; Ditchfield, R.; Pople, J. A. *J. Chem. Phys.* 1972, 56, 2257–2261.
- (37) O'Boyle, N. M.; Tenderholt, A. L.; Langner, K. M. *J. Comput. Chem.* 2008, 29, 839–845.
- (38) (a) Cossi, M.; Rega, N.; Scalmani, G.; Barone, V. *J. Comput. Chem.* 2003, 24, 669–681. (b) Barone, V.; Cossi, M. *J. Phys. Chem. A* 1998, 102, 1995–2001.
- (39) (a) Onishi, T.; Takano, Y.; Kitagawa, Y.; Kawakami, T.; Yoshioka, Y.; Yamaguchi, K. *Polyhedron* 2001, 20, 1177–1184. (b) Nagao, H.; Nishino, M.; Shigeta, Y.; Soda, T.; Kitagawa, Y.; Onishi, T.; Yoshioka, Y.; Yamaguchi, K. *Coord. Chem. Rev.* 2000, 198, 265–295. (c) Mitani, M.; Mori, H.; Takano, Y.; Yamaki, D.; Yoshioka, Y.; Yamaguchi, K. *J. Chem. Phys.* 2000, 113, 4035–4051.
- (40) (a) Hotze, A. C. G.; van der Geer, E. P. L.; Kooijman, H.; Spek, A. L.; Haasnoot, J. G.; Reedijk, J. *Eur. J. Inorg. Chem.* 2005, 2648–2657. (b) Velders, A. H.; van der Schilden, K.; Hotze, A. C. G.; Reedijk, J.; Kooijman, H.; Spek, A. L. *Dalton Trans.* 2004, 3, 448–455. (c) Das, C.; Saha, A.; Hung, C. H.; Lee, G. H.; Peng, S. M.; Goswami, S. *Inorg. Chem.* 2003, 42, 198–204. (d) Chakraborty, I.; Sengupta, S.; Das, S.; Banerjee, S.; Chakravorty, A. *Dalton Trans.* 2003, 134–140. (e) Sengupta, S.; Chakraborty, I.; Chakravorty, A. *Eur. J. Inorg. Chem.* 2003, 6, 1157–1160. (f) Hotze, A. C. G.; Velders, A. H.; Ugozzoli, F.; Biagini-Cingi, M.; Manotti-Lanfredi, A. M.; Haasnoot, J. G.; Reedijk, J. *Inorg. Chem.* 2000, 39, 3838–3844. (g) Ackermann, M. N.; Naylor, J. W.; Smith, E. J.; Mines, G. A.; Amin, N. S.; Kerns, M. L.; Woods, C. *Organometallics* 1992, 11, 1919–1926. (h) Krause, R. A.; Krause, K. *Inorg. Chem.* 1984, 23, 2195–2198. (i) Goswami, S.; Mukherjee, R.; Chakravorty, A. *Inorg. Chem.* 1983, 22, 2825–2832. (j) Krause, R. A.; Krause, K. *Inorg. Chem.* 1982, 21, 1714–1720. (k) Krause, R. A.; Krause, K. *Inorg. Chem.* 1980, 19, 2600–2603.
- (41) (a) Bersuker, I. B. *Chem. Rev.* 2001, 101, 1067–1114. (b) Köppel, H.; Domcke, W.; Cederbaum, L. S. *Adv. Chem. Phys.* 1984, 57, 59.
- (42) Kaim, W.; Kohlmann, S.; Jordanov, J.; Fenske, D. Z. *Anorg. Allg. Chem.* 1991, 598/599, 217–234.
- (43) (a) Wei, M.; Willett, R. D.; Hipps, K. W. *Inorg. Chem.* 1996, 35, 5300–5303. (b) Stange, A. F.; Waldhör, E.; Moscherosch, M.; Kaim, W. Z. *Naturforsch.* 1995, 50b, 115–122.
- (44) Takaichi, J.; Morimoto, Y.; Ohkubo, K.; Shimokawa, C.; Hojo, T.; Mori, S.; Asahara, H.; Sugimoto, H.; Fujieda, N.; Nishiwaki, N.; Fukuzumi, S.; Itoh, S. *Inorg. Chem.* 2014, 53, 6159–6169.
- (45) Boiocchia, M.; Fabbri, L. *Chem. Soc. Rev.* 2014, 43, 1835–1847.
- (46) Tomislav, P. *Acta Crystallogr., Sect. E: Struct. Rep. Online* 2006, 62, m620–m622.

- (47) Hossain, M. M.; Tseng, M.-C.; Lee, C.-R.; Shyu, S.-G. *Eur. J. Inorg. Chem.* **2014**, 36–40.
- (48) Datta, D.; Chakravorty, A. *Inorg. Chem.* **1983**, *22*, 1085–1090.
- (49) Santra, P. K.; Das, D.; Misra, T. K.; Roy, R.; Sinha, C.; Peng, S.-M. *Polyhedron* **1999**, *18*, 1909–1915.
- (50) Goswami, S.; Kharmawphlang, W.; Deb, A. K.; Peng, S.-M. *Polyhedron* **1996**, *15*, 3635–3641.
- (51) Masood, M. A.; Zacharias, P. S. *J. Chem. Soc., Dalton Trans.* **1991**, 111–114.
- (52) (a) Herebian, D.; Wiegardt, K. E.; Neese, F. *J. Am. Chem. Soc.* **2003**, *125*, 10997–11005. (b) Chaudhuri, P.; Verani, C. N.; Bill, E.; Bothe, E.; Weyhermüller, T.; Wiegardt, K. *J. Am. Chem. Soc.* **2001**, *123*, 2213–2223. (c) Herebian, D.; Bothe, E.; Bill, E.; Weyhermüller, T.; Wiegardt, K. *J. Am. Chem. Soc.* **2001**, *123*, 10012–10023.
- (53) Ye, S.; Sarkar, B.; Lissner, F.; Schleid, T.; van Slageren, J.; Fiedler, J.; Kaim, W. *Angew. Chem., Int. Ed.* **2005**, *44*, 2103–2106.